Structure and seismic hazard of the ventura avenue anticline and ventura fault, California : prospect for large, multisegment ruptures in the western transverse ranges

Hubbard, Judith; Shaw, John H.; Dolan, James; Pratt, Thomas L.; McAuliffe, Lee; Rockwell, Thomas K.

2014

Hubbard, J., Shaw, J. H., Dolan, J., Pratt, T. L., McAuliffe, L., & Rockwell, T. K. (2014). Structure and Seismic Hazard of the Ventura Avenue Anticline and Ventura Fault, California: Prospect for Large, Multisegment Ruptures in the Western Transverse Ranges. Bulletin of the Seismological Society of America, 104(3), 1070-1087.

https://hdl.handle.net/10356/104839

https://doi.org/10.1785/0120130125

THE SEISMOLOGICAL SOCIETY OF AMERICA
400 Evelyn Ave., Suite 201
Albany, CA 94706-1375
(510) 525-5474; FAX (510) 525-7204
www.seismosoc.org

Bulletin of the Seismological Society of America, Vol. 104, No. 3, pp. 1070–1087, June 2014, doi: 10.1785/0120130125

Structure and Seismic Hazard of the Ventura Avenue Anticline and Ventura Fault, California: Prospect for Large, Multisegment Ruptures in the Western Transverse Ranges

by Judith Hubbard,* John H. Shaw, James Dolan, Thomas L. Pratt, Lee McAuliffe, and Thomas K. Rockwell

Abstract The Ventura Avenue anticline is one of the fastest uplifting structures in southern California, rising at ~5 mm/yr. We use well data and seismic reflection profiles to show that the anticline is underlain by the Ventura fault, which extends to seismogenic depth. Fault offset increases with depth, implying that the Ventura Avenue anticline is a fault-propagation fold. A decrease in the uplift rate since ~30 ± 10 ka is consistent with the Ventura fault breaking through to the surface at that time and implies that the fault has a recent dip-slip rate of ~4.4–6.9 mm/yr.

To the west, the Ventura fault and fold trend continues offshore as the Pitas Point fault and its associated hanging wall anticline. The Ventura–Pitas Point fault appears to flatten at about 7.5 km depth to a detachment, called the Sisar decollement, then step down on a blind thrust fault to the north. Other regional faults, including the San Cayetano and Red Mountain faults, link with this system at depth. We suggest that below 7.5 km, these faults may form a nearly continuous surface, posing the threat of large, multisegment earthquakes.

Holocene marine terraces on the Ventura Avenue anticline suggest that it grows in discrete events with 5–10 m of uplift, with the latest event having occurred ~800 years ago (Rockwell, 2011). Uplift this large would require large earthquakes (M_w 7.7–8.1) involving the entire Ventura/Pitas Point system and possibly more structures along strike, such as the San Cayetano fault. Because of the local geography and geology, such events would be associated with significant ground shaking amplification and regional tsunamis.

Introduction

The Ventura fault is a north-dipping reverse fault that produces a monoclinal scarp running through the city of Ventura, California (Ogle and Hacker, 1969; Sarna-Wojcicki *et al.*, 1976; Yeats, 1982a; Perry and Bryant, 2002; Fig. 1). To its north lies the Ventura Avenue anticline, which houses the Ventura Avenue Oil Field, the seventh-largest oil field in California (California Department of Oil, Gas, and Geothermal Resources, 1997). Uplifted and tilted Upper Quaternary terraces on the Ventura River, which crosses the Ventura Avenue anticline, indicate that the fold has been rising at a rate of ~5 mm/yr for the last 30 ka (Rockwell *et al.*, 1988), making it one of the fastest growing anticlines in California. However, the seismogenic potential of the Ventura fault and the Ventura Avenue anticline is poorly understood due to first-order disagreements over the subsurface structure of the system.

Two models have been proposed for the Ventura system: one suggesting that the Ventura fault is a shallow, bending-moment fault that extends only about 300 m deep into the subsurface, with slip decreasing with depth (Yeats, 1982a, b; Huftile and Yeats, 1995; Fig. 2a), and an alternative interpretation that the Ventura fault extends to seismogenic depth beneath the anticline (Sarna-Wojcicki *et al.*, 1976; Sarna-Wojcicki and Yerkes, 1982; Fig. 2b). Distinguishing between these two models is essential in order to adequately describe the seismic hazard associated with this fault.

The Ventura Avenue anticline and Ventura fault are situated in a transition zone between two major north-dipping reverse faults, the San Cayetano fault to the east and the Red Mountain fault to the west. As a consequence, the Ventura system likely accommodates significant shortening. In addition, the Ventura system may link structurally to other faults

*Now at Earth Observatory of Singapore, N2-01a-07, Nanyang Technological University, 50 Nanyang Avenue, Singapore 639798, Singapore.

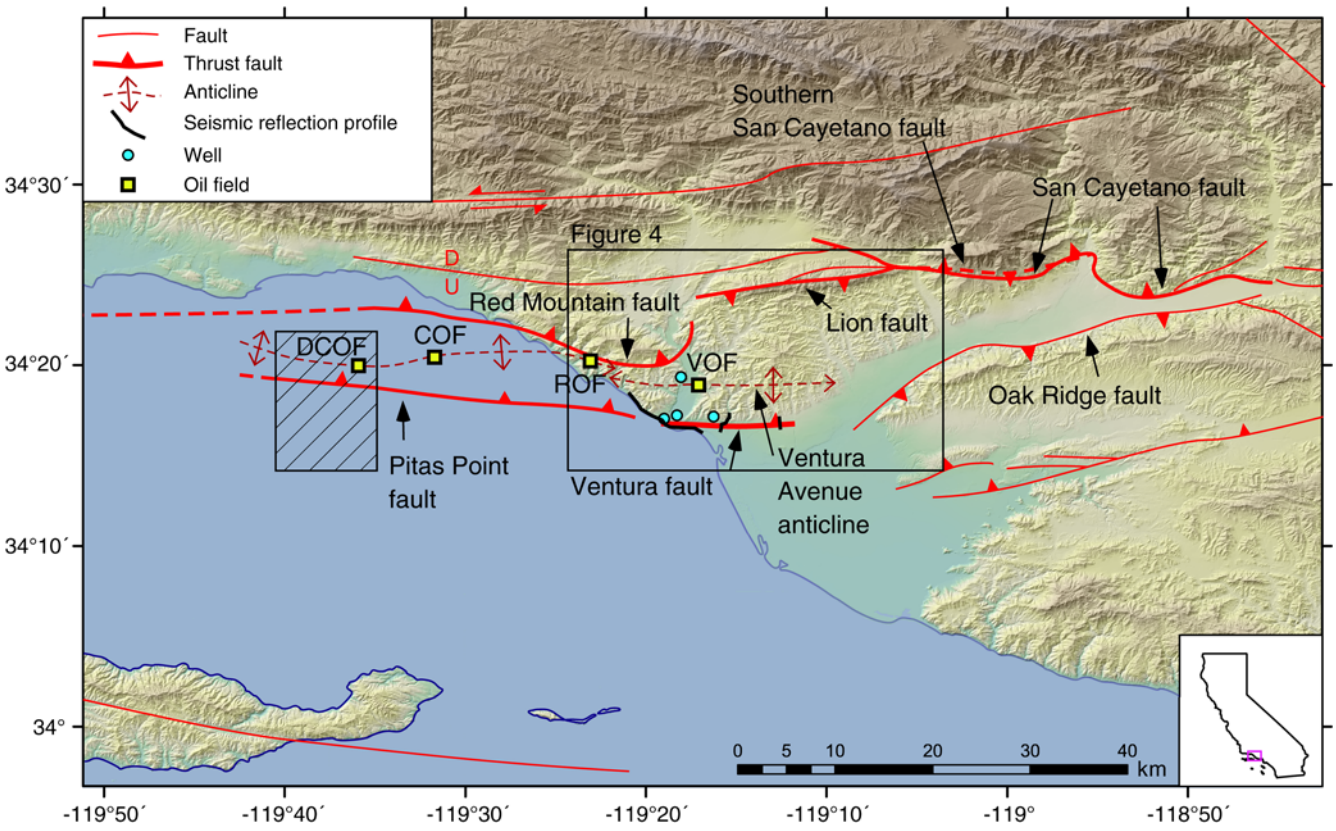

Figure 1. The Ventura region. Triangles on fault lines denote thrust fault hanging wall. The Ventura–Pitas Point fault system is called the Ventura fault (onshore) and the Pitas Point fault (offshore). Circles show the locations of wells with evidence of an intersection with the Ventura fault (see Fig. 4 for well names). Seismic reflection profiles: (left) industry line VB1, (center) Evergreen/Hall Canyon, and (right) Brookshire profile. The box with hatch marks shows the location of the 3D seismic reflection volume across the Dos Cuadras structure; from this dataset, we interpret that the Ventura–Pitas Point fault extends through, and possibly beyond, this region. The anticline in the hanging wall of the Ventura–Pitas Point fault is marked with a dashed line; oil fields along this structural trend are marked with squares: VOF, Ventura Oil Field; ROF, Rincon Oil Field; COF, Carpineteria Oil Field; and DCOF, Dos Cuadras Oil Field. North of the Ventura fault, this anticline is called the Ventura Avenue anticline. Near the trace of the San Cayetano fault, we interpret a new, previously unmapped fault that we call the southern San Cayetano fault (SSCF), shown with a dashed line; we suggest that this fault is either an eastward continuation of the Lion backthrust or a blind north-dipping thrust ramp. The color version of this figure is available only in the electronic edition.

in the region. The 1999 M_w 7.6 Chi-Chi earthquake, Taiwan, and 2008 M_w 7.9 Wenchuan earthquake, China, both demonstrate that structural linkage of thrust systems in earthquakes can result in large and damaging events (e.g., Yue *et al.*, 2005; Hubbard *et al.*, 2010; Qi *et al.*, 2011). If the Ventura system is similarly linked to other nearby faults, it may also be capable of participating in large, multisegment ruptures.

Although there are no historical earthquakes on the Ventura fault, high-resolution seismic reflection data show that it deforms upper Pleistocene and younger strata, and the fault has been mapped as offsetting a Holocene alluvial fan (Sarna-Wojcicki *et al.*, 1976). The seismic hazard associated with the Ventura fault is compounded by the fact that the region is underlain by a deep sedimentary basin that will likely amplify ground shaking during large earthquakes (Field, 2000, 2001). Thus, a better understanding of the structure of the Ventura fault, and how the fault interacts with the major faults to its east and west, is of critical importance for regional earthquake hazards assessment.

Although there have been a number of interpretations of individual datasets over the Ventura fault, there has been no integrated interpretation of all of these data. Here, we reinterpret all of the available datasets bearing on the Ventura fault, add new information from previously unpublished industry seismic profiles, collect new high-resolution seismic profiles over the fault tip within the urban area, and use these constraints to develop a subsurface model for the Ventura fault. We then use this model as a basis for estimating fault slip. This paper thus presents a kinematic model that is consistent with available and new data and then uses this model to estimate slip rates as constrained by measured uplift rates.

Geometry of the Ventura Fault

We use a comprehensive set of petroleum well data, industry seismic reflection profiles, and two seismic reflection profiles acquired by our group in August 2010 to construct a more complete 3D model of the Ventura fault system.

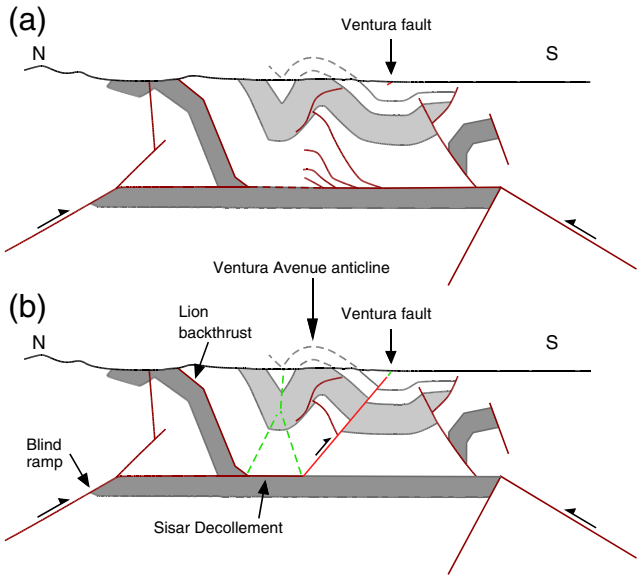

Figure 2. Schematic north–south cross sections showing alternate models for the Ventura Avenue anticline and Ventura fault. (a) Cross section after Yeats (1982a) and Huftile and Yeats (1995). In this model, the Ventura Avenue anticline is a north-vergent detachment fold lifting off of the Sisar decollement; minor faulting in the interior of the anticline is constrained by well data. The Ventura fault is a minor bending-moment fault in the syncline at the southern edge of the anticline. (b) Our interpretation, modeled in part after Sarna-Wojcicki and Yerkes (1982). The Ventura Avenue anticline is produced as a consequence of shortening on the Ventura fault, which is a steeply dipping south-vergent thrust fault rising from the Sisar decollement. Slip on the blind ramp to the north is partitioned between the Lion backthrust and the Ventura fault. The color version of this figure is available only in the electronic edition.

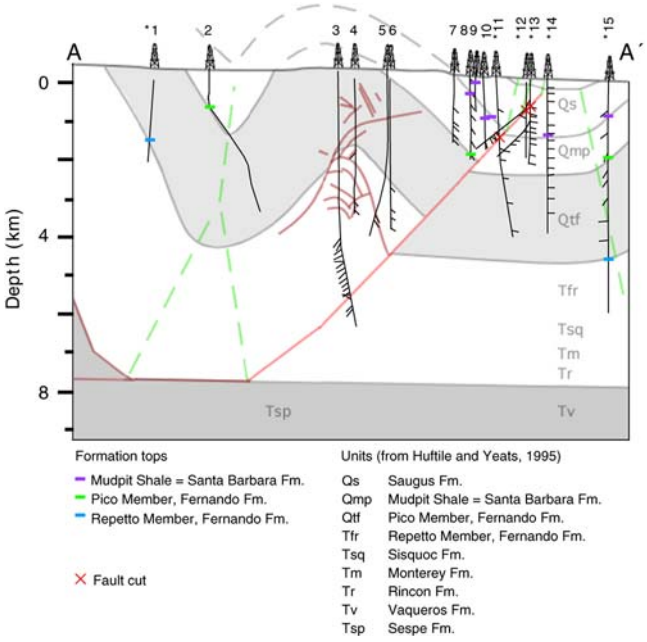

Figure 3. Cross section of the Ventura Avenue anticline and Ventura fault showing a subset of the well data. Cross section is after Huftile and Yeats (1995), modified to match our interpretation of a deeply rooted Ventura fault. Asterisks indicate that the well has not been projected directly, but rather shifted along strike to its location relative to the Ventura fault; this allows us to show wells that are farther from the cross section. The API numbers of the wells (unique identifiers) are 1 = 11121309; 2 = 11120035; 3 = 11120458; 4 = 11105289; 5 = 11120851; 6 = 11103876; 7 = 11105923; 8 = 11105917; 9 = 11104005; 10 = 11105919; 11 = 11104006; 12 = 11105811; 13 = 11106169; 14 = 11120500; 15 = 11105798. For locations of wells and cross section, see Figure 4. There is no vertical exaggeration. The color version of this figure is available only in the electronic edition.

Previous studies of the Ventura fault and Ventura Avenue anticline have relied primarily on well data (e.g., Sarna-Wojcicki and Yerkes, 1982; Yeats, 1982a,b; Huftile and Yeats, 1995). Such studies have been limited to 2D cross-sectional analyses, neglecting lateral variations in geometry across the anticline. In addition, some wells were mislocated by as much as 200 m, a distance that is especially significant given the steep dip (45°–55° N) that we, and others (Yerkes *et al.*, 1987), interpret for the Ventura fault. In contrast, our 3D analysis allows us to consider all constraints in a single, comprehensive model.

Data and Observations

We take petroleum well data from published papers arguing both for (e.g., Sarna-Wojcicki and Yerkes, 1982) and against (e.g., Yeats, 1982a,b) the existence of a major fault underlying the Ventura Avenue anticline and incorporate them into our 3D model of the system. We add well data extracted from California's Department of Conservation online well database (see Data and Resources). Figure 3 shows a schematic cross section with wells; see Figure 4 for mapped locations. In addition, our model incorporates an industry seismic reflection profile that images the fault, two seismic

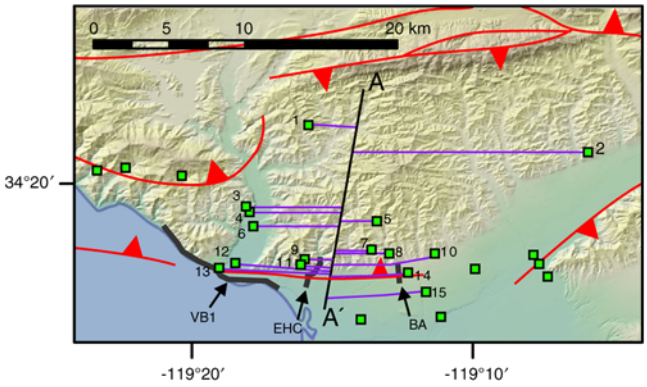

Figure 4. Locations of wells (squares) and seismic reflection profiles (lines VB1, EHC, BA) used to constrain the cross section across the Ventura Avenue anticline. The well numbers are translated to API numbers in the caption of Figure 3. Lines connecting squares to AA′ show how wells are projected onto the cross section. VB1, industry seismic reflection profile (Fig. 5); EHC, Evergreen/Hall Canyon profile; BR, Brookshire Avenue profile (Fig. 6). The location of the cross section is the same as cross section BB′ of Huftile and Yeats (1995). Note that some of the wells are projected on curved lines to allow for the curvature of the range front. The color version of this figure is available only in the electronic edition.

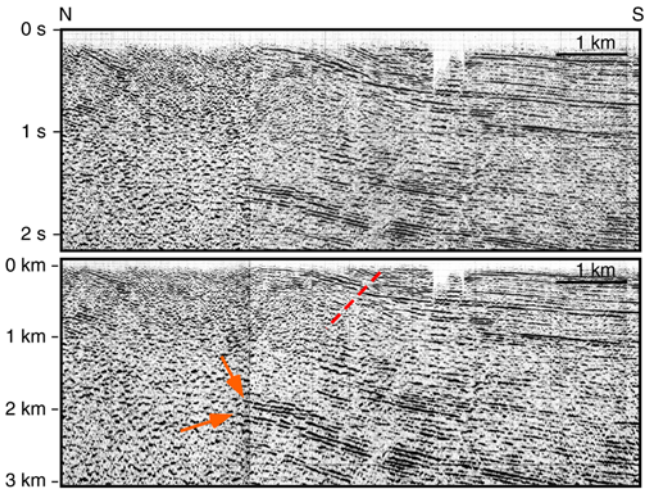

Figure 5. Portion of industry seismic reflection profile VB1, which images the Ventura fault; (top) in two-way travel time and (bottom) in depth (converted using the 1D velocity model of Brankman, 2009). Arrows point to prominent reflector terminations; dashed line marks interpreted fault surface, with dipping reflectors in the hanging wall and nearly horizontal reflectors in the footwall. No vertical exaggeration is shown in the bottom image. The color version of this figure is available only in the electronic edition.

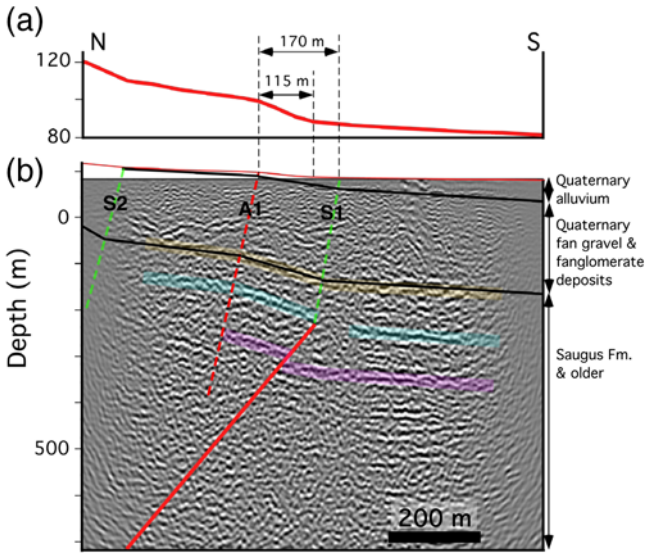

Figure 6. High-resolution seismic reflection profile along Brookshire Avenue, acquired August 2010; see Figure 1 for location. Stratigraphic units are projected from the geological map (Dibblee and Ehrenspeck, 1992). (a) Topographic profile; note the clear scarp. (b) Seismic profile with interpretation; the solid line shows the Ventura fault. The monocline associated with the fault tip consists of a coupled anticline (axial plane denoted by dashed line A1) and syncline (axial plane denoted by dashed line S1). (An additional synclinal axial surface, S2, associated with the southern extent of the Ventura Avenue anticline is also shown.) Syncline S1 is connected to the fault tip, which lies ~230 m.b.s.l. The syncline appears to lie ~55 m to the south of the base of the scarp, and is likely covered by ~5 m of sediments. No vertical exaggeration is shown. The color version of this figure is available only in the electronic edition.

profiles collected by our group in August 2010, and various geological maps.

Our key observations and constraints on the Ventura fault include the following:

1. the surface map of the fault scarp (Dibblee and Ehrenspeck, 1988, 1992);
2. an industry seismic reflection line that crosses the Ventura fault at its western subaerial extent (Fig. 5), acquired along the coastline (Fig. 1; see Data and Resources for details) and depth-converted using the 1D velocity model of Brankman (2009);
3. two shallow seismic reflection profiles, which we acquired in August 2010 using a Vibroseis source, along Brookshire Avenue and Evergreen Drive/Hall Canyon Road in the city of Ventura (Figs. 1 and 6);
4. two dipmeter logs that show changes in dip at the interpreted fault or dip panels that otherwise constrain the fault depth (Fig. 7a,b; Table 1; one well shows evidence of stratigraphic repetition at the fault);
5. one interpreted fault based on ~245 m of repeated section (Fig. 7c); and
6. one discontinuity in a conductivity log that correlates with the interpreted fault (Fig. 7d; Table 1).

The geomorphic scarp associated with the Ventura fault has been described at various locations along strike by Putnam (1942), Ogle and Hacker (1969), Quick (1973), Nichols (1974), and Sarna-Wojcicki *et al.* (1976); see the United States Geological Survey (USGS) fault database, Data and Resources, for a summary. It is a north-dipping reverse-oblique slip fault visible at the surface as an east–west-trending monoclinal scarp and extends approximately 14 km through the city of Ventura.

The industry seismic reflection profile, VB1, provides the clearest image of the Ventura fault (Fig. 5). This line was acquired along the coastline at an oblique angle to the structure in the area (Fig. 1). Near the projected surface trace of the Ventura fault, we observe a distinct fold axis in the upper 500 m, separating a south-dipping panel to the north from shallowly dipping reflectors to the south (fold axis marked with a dashed line in Fig. 5). The reflectors above 200 m appear to be continuously folded across this fold axis or have offsets that are too small to be resolved on the seismic data (less than ~20 m). However, at greater depths, between 200 and 500 m below sea level (m.b.s.l.), reflectors are offset with reverse displacement. At 2.0 km below sea level (km.b.s.l.), we note the presence of several major reflectors that terminate abruptly along the down-dip projection of the fault below the southern limb of the anticline.

The truncated reflectors visible in the industry line are interpreted as footwall cutoffs (Fig. 5), whereas the offset reflectors at 200–500 m.b.s.l. are interpreted as paired hanging wall and footwall cutoffs that constrain both the fault location and amount of dip-slip displacement (Figs. 5 and 6). The uppermost reflector that appears to be folded, but not

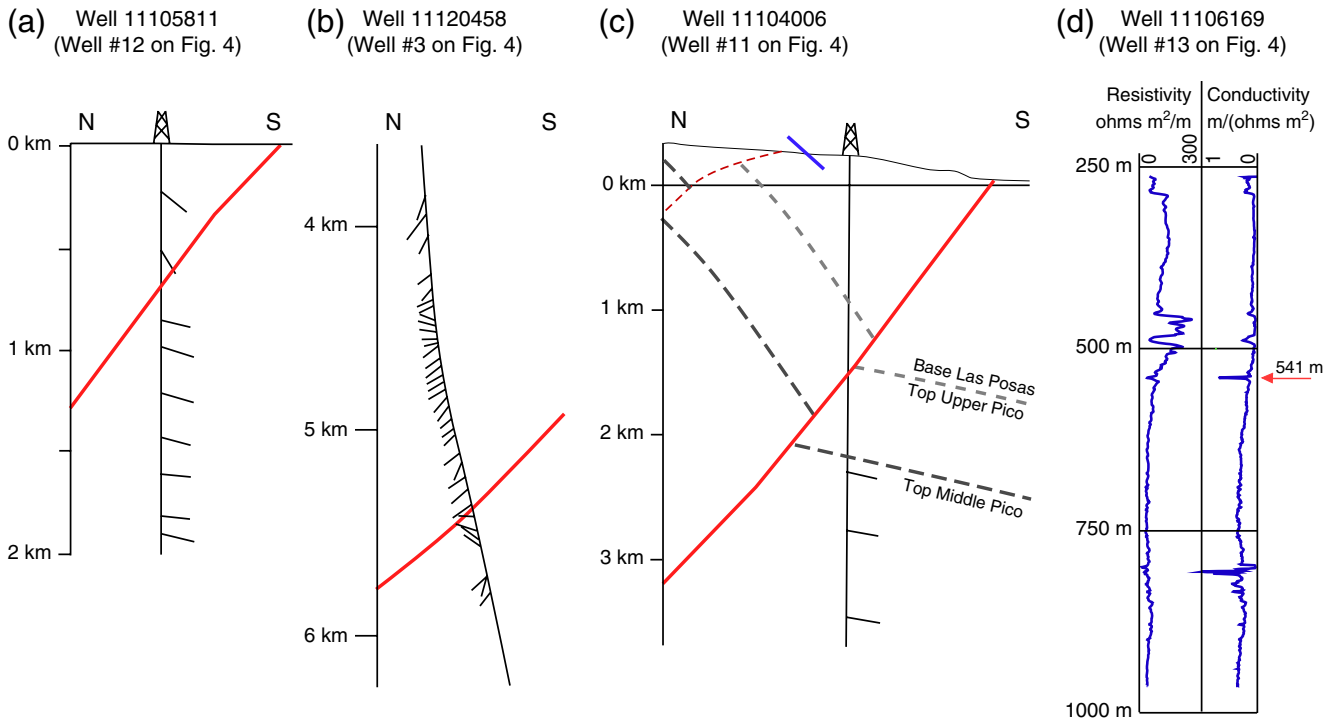

Figure 7. Well logs showing interpreted fault intersections for the Ventura fault. (a) Dip data for well 11105811. The cross-cutting line indicates the interpreted Ventura fault. Dip data and suggested fault intersections from Figure 1 of Sarna-Wojcicki and Yerkes (1982). Yerkes *et al.* (1987) estimate vertical throw of 150–200 m in this well. (b) Dip data for well 11120458; note the change in dips at the projected fault location. The cross-cutting line shows the location of the interpreted Ventura fault. Dip data taken from figure 3 of Yeats (1983). (c) Dip and formation data for well 11104006. Data taken from Ogle and Hacker (1969); fault dip shallowed slightly to match our interpretation. The surface dip measurement from Dibblee and Ehrenspeck (1988) is shown to the left of the well. Ogle and Hacker (1969) observe ~245 m of repeated section in this well. (d) Conductivity and resistivity profiles for well 11106169. The arrow indicates a spike in conductivity and drop in resistivity, which matches the modeled fault location. The color version of this figure is available only in the electronic edition.

offset, implies that the structure terminates upward into a synclinal fold within a few hundred meters of the surface. Alternatively, at less than 200 m.b.s.l., the fault may have such small displacement that it cannot be resolved on the industry profile.

The results of our August 2010 field survey are consistent with the structure imaged in the industry seismic line VB1. Line VB1 shows a monoclinal panel bounded by parallel synclinal and anticlinal axial surfaces within the upper 500 m (Fig. 8). The 2010 field survey, together with published trenches across the scarp (Sarna-Wojcicki *et al.*, 1976; Yeats, 1982a), demonstrates that the subsurface monocline extends to the eastern edge of the mapped fault trace (Figs. 1 and 6). At line VB1, this monocline is about 500 m wide, whereas at Brookshire Avenue, the high-resolution seismic line shows that it is ~170 m wide (Fig. 6; see Fig. 1 for location). The topographic scarp is not present at line VB1 due to fluvial and marine erosion, but the Brookshire Avenue profile indicates that where the surface scarp is present, the top of the scarp roughly corresponds to the anticlinal axial surface imaged in the subsurface. The same high-resolution line shows that the synclinal axial surface at the base of the monocline lies ~55 m to the south of the surface scarp (Fig. 6). Thus, we interpret this to indicate that the scarp may be partially obscured by Holocene deposits. This is consistent with observations from a trench across the Ventura

Table 1
Wells Used to Constrain the Geometry of the Ventura Fault

API Well Number	Latitude (°)	Longitude (°)	Fault Depth (m.b.s.l.)	Source
11104006	34.28689	−119.26942	1356	Ogle and Hacker (1969), Sarna-Wojcicki *et al.* (1976), and Yeats (1982a)
11105811	34.28543	−119.30609	700	Sarna-Wojcicki and Yerkes (1982) and Yerkes *et al.* (1987)
11106169	34.28368	−119.31691	541	This study
11120458	34.32116	−119.30173	5320	Observation from Yeats, 1983; reinterpreted in this study

Latitude and longitude are for the location of the fault at depth, not for the well at the surface; these differ for nonvertical wells. See Figure 7 for fault intersection evidence based on well data.

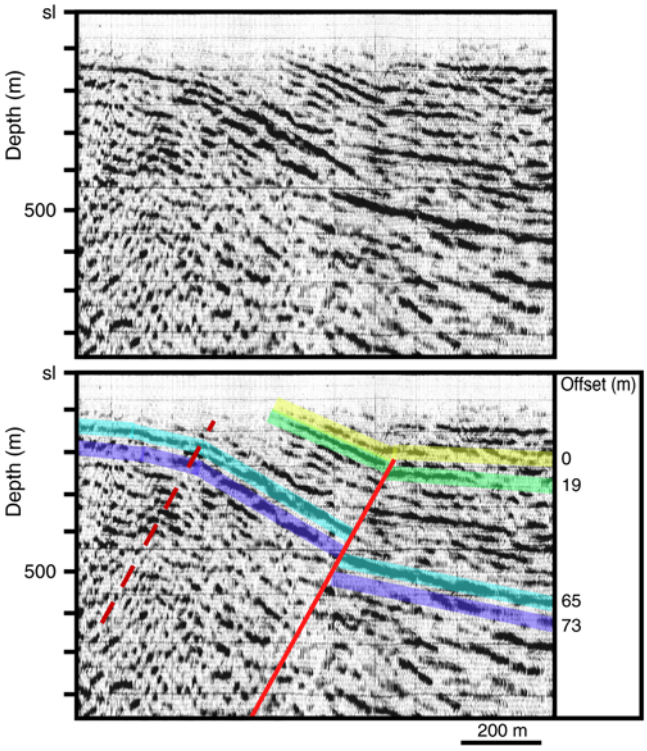

Figure 8. Fault displacement on the Ventura fault, as mapped on industry seismic line VB1. Displacement decreases toward the tip and does not reach the surface. The dashed line marks the anticlinal axial surface on the northern side of the monocline. Note that in this image, line VB1 has been depth-converted and projected onto a line perpendicular to the structural trend to correct for the fact that the line was originally acquired at an oblique angle to the structure. No vertical exaggeration is shown. The color version of this figure is available only in the electronic edition.

fault scarp, which showed an inferred paleosol that extends beneath the base of the topographic scarp at a steeper dip than topography (Ventura County Hospital Trench; fig. 5 of Sarna-Wojcicki *et al.*, 1976).

The seismic and geomorphic constraints are all consistent with the presence of a steep, north-dipping Ventura fault that extends to at least 2 km.b.s.l (the deepest reach of the available data) and has enough slip to generate a several-hundred-meter-wide fold panel at its tip. Collectively, these constraints indicate that the fault dips approximately 45°–55° to the north. This steep dip is consistent with the geometry suggested by Ogle and Hacker (1969) and Sarna-Wojcicki and Yerkes (1982).

The geometry of the fault is further constrained by petroleum wells drilled within the Ventura Avenue anticline. The large majority of wells in the region are located along the crest of the Ventura Avenue anticline and are not deep enough to reach the Ventura fault, as indicated by the seismic lines. However, several wells drilled along the southern limb of the anticline provide important constraints on the structure at depth, including dipmeter logs, stratigraphic horizon tops, and electrical conductivity logs. We incorporate wells shown in published cross sections in addition to supplementary wells extracted from California's Department of Conservation online well database in our 3D model.

Four wells show evidence of a possible Ventura fault (Table 1; Fig. 7). Two wells (API 11105811 and 11120458) show abrupt changes in dip at the projected fault location; Yerkes *et al.* (1987) also estimate vertical throw of 150–200 m on well 11105811 (Fig. 7a,b). A third well shows stratigraphic repetition: well 11104006 exhibits apparent vertical separation of 245 m of the Pleistocene Las Posas Formation (Ogle and Hacker, 1969; Fig. 7c). We have identified a fourth well (API 11106169) that shows a discontinuity in conductivity at a level consistent with the projected fault depth, which we suggest may be due to either fluid accumulation on the fault surface or failure of the logging tool in the core of the fault-damaged rock zone (Fig. 7d).

Although most of these fault intersections are located within the upper 2 km, like the evidence of faulting from the seismic lines, the inferred well cut in well 11120458 is located much deeper, exhibiting a distinct discontinuity in dips at ~5320 m.b.s.l. Dips above this level are consistently about 30°–50° to the north, whereas dips below are to the south and become more variable. This discontinuity occurs at the down-dip projection of the fault. Although such a change in dip pattern does not require the presence of a fault, such changes are often associated with faults (e.g., Devilliers and Werner, 1990; Adams *et al.*, 1992), and here the location and style of the change is consistent with the down-dip projection of a planar Ventura fault. Alternatively, these dip changes could reflect small-scale folding and faulting in the hanging wall of the Ventura fault, with the fault passing somewhere below the lowermost south-dipping beds. A folding interpretation of these deviated dips would imply that the Ventura fault dips 3°–4° more steeply than shown in our primary interpretations.

Modeling

In order to construct a complete 3D fault model, all of these data and constraints, including geological maps, fault intersections from wells, and seismic profiles, were georeferenced and integrated into Gocad (Mallet, 1992), a 3D computer-aided design tool. We then built a triangulated surface representation of the fault following the approach of Plesch *et al.* (2007). The eastern extent of the fault is defined by the mapped surface trace together with the mapped extent of the Ventura Avenue anticline; to the west, the Ventura fault must extend at least to line VB1, along the coast.

When all of the well and seismic observations are considered in their precise subsurface locations, they can be fit by a single, nearly planar surface that dips 45°–55° to the north beneath the Ventura Avenue anticline (Fig. 9). The deepest interpreted fault constraint is at 5320 m.b.s.l.; however, the geometry of the Ventura Avenue anticline suggests the fault extends deeper. Specifically, the north dip of the fault where it is constrained by the well and seismic data

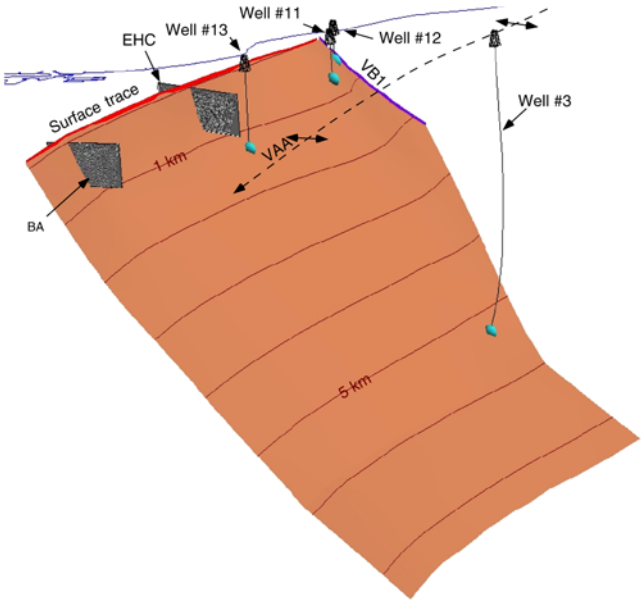

Figure 9. Perspective view of the Ventura fault model from the east-northeast, with data constraints as shown; 1 km depth contours are marked. (VAA, surface trace of the Ventura Avenue anticline; VB1, fault pick from that line.) The ovals below each well show fault picks from wells; well numbers are the same as in Figures 3 and 4. EHC and BA are seismic profiles collected in August 2010 (Evergreen/Hall Canyon and Brookshire Avenue, respectively). The thin line marks the coastline. The color version of this figure is available only in the electronic edition.

is parallel to the backlimb of the Ventura Avenue anticline. In standard fault-related folding theories (Suppe, 1983; Suppe and Medwedeff, 1990; Shaw *et al.*, 2005), this geometry implies that the fault continues to depth beneath the fold limb and that the intersection of the fault and the synclinal axial surface at the northern limit of the fold defines the base of the fault ramp, where the fault flattens to a detachment (Fig. 3). We interpret this fault bend to occur at ~7400 m.b.s.l., consistent with the level of the Sisar decollement, which is either horizontal (e.g., Huftile and Yeats, 1995) or dips gently to the north.

Slip and Activity of the Ventura Fault

The Ventura Avenue anticline began to develop in the Quaternary, after the deposition of the uppermost Saugus Formation. This formation, which is estimated to be 250 ± 50 ka (based on amino-acid racemization on fossil mollusks; Wehmiller *et al.*, 1978; Lajoie *et al.*, 1982, 1991; Yerkes *et al.*, 1987), is well stratified within the anticline and lacks angular unconformities (Lajoie *et al.*, 1982), indicating that deposition of the Saugus Formation predates folding of the anticline. River terraces, which are both uplifted and tilted, provide constraints on the development of the anticline (Rockwell *et al.*, 1988), suggesting that folding continued through the late Pleistocene (Fig. 6). This is consistent with the high-resolution seismic data we acquired across the tip of the Ventura fault, which shows deformed late Pleistocene and younger strata (Fig. 6). Finally, the fault scarp has been mapped as offsetting the Harmon Canyon alluvial fan (5.7–15 ka; Sarna-Wojcicki *et al.*, 1976; Clark *et al.*, 1984), implying that the fault system remains active.

Uplifted terraces cut into the Ventura Avenue anticline provide a measure of vertical deformation rates over time (Lajoie *et al.*, 1982; Rockwell *et al.*, 1988). More recent exposure dating provides consistent dates for terrace F, which represents geomorphic surface Qt6a of Rockwell *et al.* (1984) (DeVecchio *et al.*, 2012). These terraces show that the anticline has been rising at a rate of ~3.0–6.9 mm/yr for the last ~30 ka, with even faster rates prior to that (up to 8.6–25.2 from 250 ± 50 to 105 or 80 ka; Table 2). Deriving a slip rate on the Ventura fault based on these vertical uplift rates on the associated anticline requires an understanding of the geometry and kinematics of the system at depth.

Kinematics

To address the geometry and kinematics of the Ventura fault and its hanging wall anticline, we measure dip-slip amounts on the fault from two data sources: (1) reflectors correlated across the fault on seismic reflection profile VB1 (Fig. 8) and (2) stratigraphic offset in wells. We observe from

Table 2
Interval Rates of Uplift and Shortening across the Ventura Avenue Anticline

Geomorphic Surface Interval	Age Interval (ka)		Interval Uplift Amount (m)	Uplift Rate (mm/yr)	Shortening Rate (mm/yr)	
					45° dip	55° dip
Bedrock (top Saugus)–H	250 ± 50	105 or 80	2145 ± 250	8.6–25.2	6.1–17.8*	5.2–15.4*
H–F	105 or 80	38 ± 1.9	440 ± 110	4.8–13.7	3.4–9.7*	2.9–8.4*
F–E	38 ± 1.9	29.7 ± 1.25	54 ± 20	3.0–14.4	2.1–10.2*	1.8–8.8*
E–B	29.7 ± 1.25	15.9 ± 0.2	65.5 ± 20	3.0–6.9	4.2–9.8†	3.7–8.4†
B–present	15.9 ± 0.2	0	67.5 ± 10	3.6–4.9	5.1–6.9†	4.4–6.0†

B, E, F, and H are terraces discussed in Rockwell *et al.* (1988). Uncertainties on ages and uplift amounts are from Rockwell *et al.* (1988), except for the uncertainty on the age of the top Saugus Formation, which is taken from Huftile and Yeats (1995). Calculations are shown for a fault dip of 45° or 55° (see Fig. 11 for equations). Uncertainty calculations take the largest possible range in ages and uplift amounts. Calculations for different fault dip are kept separate, as fault dip remains constant through time.

*Shortening rate calculated based on fault-propagation fold model.

†Shortening rate calculated based on fault-bend fold model.

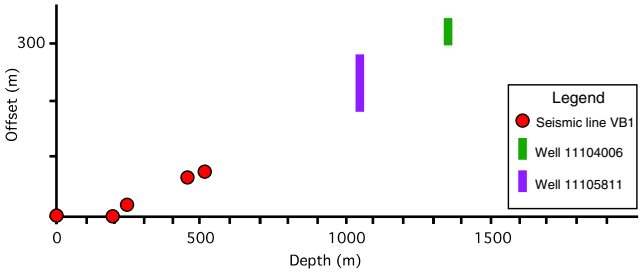

Figure 10. Graph depicting increasing offset with depth on the Ventura fault. Depth is measured on the footwall, in m.b.s.l.; the legend shows the sources of measurements. Note that the measurements from wells 11105811 and 11104006 represent 150–200 m and 245 m of vertical throw (from Yerkes *et al.*, 1987, and Ogle and Hacker 1969, based on stratigraphic repetition), converted to 173–230 m and 299–346 m of slip on a 45°–55° dipping fault, respectively. The color version of this figure is available only in the electronic edition.

line VB1 that in the upper 200 m, reflectors appear continuous. However, below 200 m, the reflectors are distinctly offset, and the amount of fault offset increases with depth, from no visible offset at 200 m.b.s.l. to ~73 m of offset at ~500 m.b.s.l. (Fig. 8). Figure 10 compares depth and fault displacement for offset reflectors from line VB1 and two published measures of fault offset determined from nearby wells. The result is a linear trend, to a maximum fault offset of ~300–350 m at ~1350 m.b.s.l. (Fig. 10). The observation of fault slip increasing linearly with depth is consistent with the displacement patterns of fault-propagation folds (Suppe and Medwedeff, 1990; Erslev, 1991; Allmendinger, 1998; Hughes and Shaw, 2012). Thus, we interpret the Ventura Avenue anticline as having formed as a fault-propagation fold in the hanging wall of the Ventura fault. The alternative, bending-moment fault model of Yeats (1982a,b) would instead require fault offset to decrease with depth, to zero offset at ~300 m.b.s.l.

We next explore a constant-thickness fault-propagation fold model (Suppe and Medwedeff, 1990; Hughes and Shaw, 2012) to assess whether the known geometry and timing of uplift across the Ventura Avenue anticline are consistent with this interpretation (Shaw *et al.*, 2005; Hughes and Shaw, 2012). In this model, we neglect the tilting observed in the river terraces; thus, this end-member model can explain most, but not all, of the deformation that we observe, as discussed in the Slip Rates and Shortening section. Fault-propagation folds form as faults propagate toward the surface over time, accommodating shortening by a combination of fault displacement and folding. Propagating faults typically show increasing offset with depth because the fold consumes slip on the fault ramp, producing zero offset at the fault tip and the greatest offset at the ramp base. The constant-thickness model for fault-propagation folds is a kinematic model that assumes angular fold hinges and conservation of bed length (Fig. 11a; Suppe and Medwedeff, 1990). In such a model, the fault propagates upward from a fault bend, and

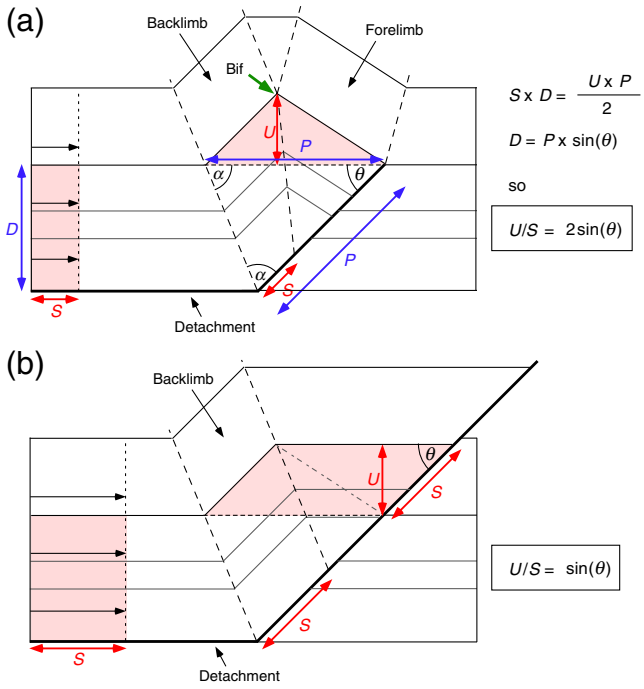

Figure 11. Kinematic models of (a) a constant-thickness fault-propagation fold (Suppe and Medwedeff, 1990; Shaw *et al.*, 2005) and (b) a fault-bend fold (Suppe, 1983; Shaw *et al.*, 2005), showing how uplift is related to slip. As required by the constant thickness model, the fault tip in (a) is located at the stratigraphic level of the bifurcation of the anticline (Bif). Note that in each of these cases, the detachment is parallel to the beds, and therefore the fault ramp is parallel to the beds in the backlimb, which requires that the slip on the fault ramp equal the slip on the detachment. Because each of these models conserves area, we can calculate the ratio of uplift to slip; we determine that this ratio is exactly twice as high in case (a) as in case (b). *S*, slip; *D*, vertical distance between detachment and fault tip; *U*, maximum uplift; *P*, length of fault ramp in fault propagation model; θ, dip of fault ramp. The color version of this figure is available only in the electronic edition.

an active syncline develops at the fault tip. As the fault propagates upward, material folds up into the forelimb. In addition, an anticline develops, and material moves progressively up the fault into the backlimb. The bifurcation point of the backlimb (i.e., the location where the anticlinal axial surface splits into two) is at the same stratigraphic level as the tip of the propagating fault (Fig. 11a). The backlimb develops like a fault-bend fold, but with a limb width that is greater than the fault slip. Here, we use a model in which the detachment is parallel to regional bedding, and thus the backlimb of the anticline is parallel to the fault. In this particular case, the fault-propagation fold will produce an uplift rate that is exactly twice that of a fault-bend fold for a given shortening rate (Fig. 11a; Suppe and Medwedeff, 1990; Shaw *et al.*, 2005).

We develop our structural model (Fig. 12) using the geometry of the Ventura fault constrained by subsurface well and seismic data, with fault slip constrained by the terrace uplifts estimated by Rockwell *et al.* (1988) (Table 2). Our model shows the development of the forelimb of the deep,

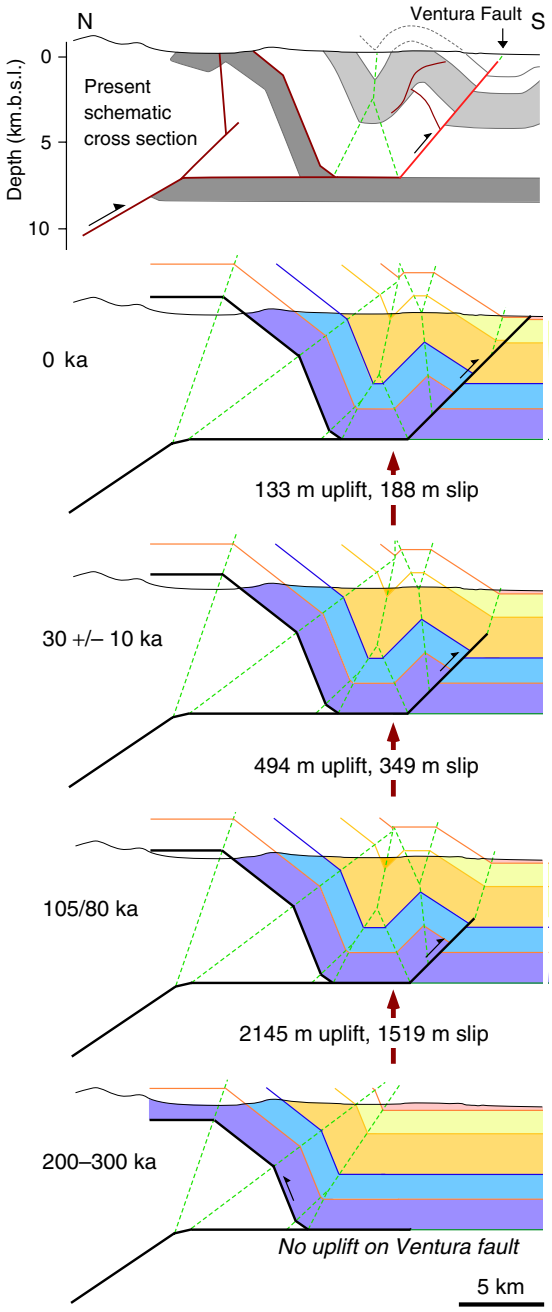

Figure 12. Kinematic model of the Ventura Avenue anticline, showing deformation over time. Uplift amounts are derived from terrace data (Rockwell *et al.*, 1988). Growth of the anticline began at 200–300 ka and continues at present. From 200–300 ka to 30 ± 10 ka, we model the anticline as a constant-thickness fault-propagation fold generated by slip and propagation of the Ventura fault. From 30 ± 10 ka to present, we model the system as a breakthrough fault-propagation fold (i.e., where the fault was slowly propagating up-dip but suddenly broke through to the surface), where the Ventura fault now extends toward the surface south of the anticline. At breakthrough, the structural behavior of the system changes to that of a fault-bend fold. Secondary faults within the anticline shown in the present-day cross section have been documented by drilling and are interpreted to accommodate tightening of the fold. For names of the features shown here, compare the uppermost cross section to Figure 2. The color version of this figure is available only in the electronic edition.

blind ramp that lies north of the intersection between the Ventura fault and the Sisar decollement, which is responsible for the uplifted terrain to the north of the Ventura Avenue anticline. At fault initiation, displacement begins to propagate southward on the Sisar decollement and onto the newly formed Ventura fault. The Ventura Avenue anticline starts to develop as a fault-propagation fold with nearly symmetric, steeply dipping fold limbs. Rockwell *et al.* (1988) identified a major decrease in uplift rate at 30 ± 10 ka, around the time that terrace E was formed (29.7 ka). Our model explains this decrease in uplift rate of the fold by breakthrough of the Ventura fault (i.e., rather than propagating slowly to the surface, the fault broke through to the surface very quickly and became surface emergent). Prior to breakthrough, uplift of the anticline included components of faulting (translation) and folding. However, after breakthrough, the uplift is due exclusively to translation on the fault and related fault-bend folding (Fig. 11b).

The model closely reproduces our basic understanding of the geometry of the Ventura Avenue anticline and the Ventura fault (Fig. 12). Moreover, this two-phase development of the anticline, with fault breakthrough at 30 ± 10 ka, reproduces the scarp that is located several hundred meters south of the main south-dipping limb of the anticline. Despite the wide range of fault-propagation fold models (e.g., Jamison, 1987; Chester and Chester, 1990; Mitra, 1990; Suppe and Medwedeff, 1990; Erslev, 1991; Mosar and Suppe, 1992; Hardy and Ford, 1997; Allmendinger, 1998), none of them provide for the existence of such a feature without fault breakthrough.

Slip Rates and Shortening

Using this model, we can calculate the shortening rate across the Ventura Avenue anticline by applying the equations derived in Figure 11. Our results, with uncertainties, are shown in Table 2. Although most of these measurements, including uncertainties, come from Rockwell *et al.* (1988), we re-evaluate the age of the bedrock surface (the top of the Saugus Formation), which Rockwell *et al.* (1988) take to be 200 ka. The Saugus Formation is poorly defined and known to be regionally diachronous, making local age estimates difficult (DeVecchio *et al.*, 2012). Here, we use the range of ages provided by Huftile and Yeats (1995), who indicate the age of the top Saugus is uncertain and could range from 200 to 300 ka or more.

Our calculations (Table 2) show the uplift rate has indeed changed over time, as the permissible rates do not fully overlap, even with generous error estimates. However, when we apply our breakthrough model, we determine that although the uplift rate must have varied, the shortening rate could have remained constant over time since fault initiation, with a rate somewhere between 5.2 and 6.9 mm/yr. Given the age uncertainties, we cannot exclude the possibility that the shortening rate may have varied over time, but this variation is not required by the data. Without the change

to breakthrough kinematics at 30 ± 10 ka, a constant shortening rate with variable uplift rate would not be viable.

We also note from these calculations that a breakthrough did not have to occur at 29.7 ka; this date simply represents the age of terrace E. We can maintain a constant shortening rate even while allowing the time of the breakthrough to vary by ±10 ka. Such a variation would still be consistent with the observed geometry of the Ventura Avenue anticline and the scarp near the fault tip.

Thus, our model explains the presence and location of the Ventura fault scarp, the fold geometries, and the uplift rates over the last 200–300 ka without requiring a variable shortening rate. The simple nature of this model, however, means that it does not explain some other detailed aspects of the structure. For example, the model does not account for the measured changing tilt rate of the anticline limbs (Rockwell *et al.*, 1988), which implies the structure grew with a component of limb rotation (in which fold limbs rotate progressively through time) together with kink-band migration (in which fold limbs widen through time while maintaining a fixed dip) (e.g., Scharer *et al.*, 2006). This observation suggests that some detailed aspects of the structure may be better explained by a fault-propagation fold model, such as trishear, that includes limb rotation (Erslev, 1991; Hardy and Ford, 1997; Allmendinger, 1998), or by including a component of detachment folding, as suggested by Yeats (1982a). However, this complexity does not affect our conclusion about breakthrough or impact our discussion below regarding the current state of deformation, as the structural kinematics of the different fault-propagation models are all similar after breakthrough (Shaw *et al.*, 2005). Finally, we note that the fault tip after breakthrough may remain ~200–300 m.b.s.l. This would suggest that the fault remains blind, being buried by young sediments in the uppermost layers and having its slip consumed by the monoclinal fold in the hanging wall that underlies the surface scarp. In any event, the shifting of the fault tip southward as a consequence of breakthrough (see Fig. 12) explains the change in uplift rate of the Ventura Avenue anticline and the scarp that lies south of the range front in the city of Ventura.

The interpreted fault geometry and kinematic model allows us to directly convert the uplift rate measured from terraces for the last 30 ka into a slip rate on the Ventura fault. After fault breakthrough, the uplift rate should represent simple translation above the fault, as shown in Figure 11b, and the shortening rate across the structure should equal the slip rate, as the detachment that links to the Ventura fault is bed parallel. Our calculations in Table 2 show the results for fault dips of 45° and 55°; this yields a slip rate of ~4.4–6.9 mm/yr for the upper segment of the Ventura fault in the last 30 ± 10 ka (the slip rate here is identical to the shortening rate shown in Table 2, as we model the detachment as horizontal). This value is significantly higher than previous measures of slip rate on this fault, which have ranged from 0.2 to 2.4 mm/yr (see the USGS fault database, Data and Resources). These faster rates appear consistent with data collected

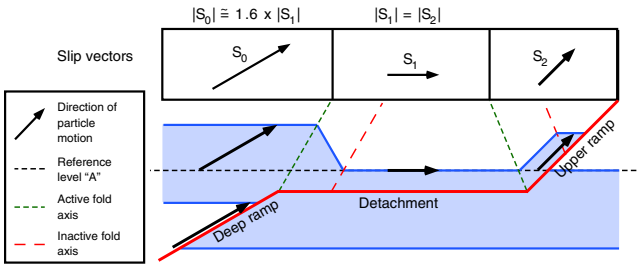

Figure 13. Schematic illustration showing how the slip vectors change in a ramp–flat–ramp fault geometry. Dashed lines show active fold axes (across which the slip vectors change) and inactive fold axes (which have been passively transported from the fault bends). Reference level A marks the original, undeformed bedding geometry. In this case, the magnitude of slip on the deep ramp is ~1.6 times that on the detachment, because slip is consumed by folding across the fault bend. In contrast, slip is neither consumed nor generated at the second fault bend because this is a special case in which the beds are parallel to the detachment and therefore parallel to the upper ramp. The geometry shown here is simpler than the Sisar–Ventura case because the lower ramp merges directly onto the detachment rather than via multiple bends. See pages 17–18 of Shaw *et al.* (2005) for details. The color version of this figure is available only in the electronic edition.

at Global Positioning System (GPS) stations in the vicinity of the Ventura fault, which show significant shortening across the region (7–10 mm/yr; Donnellan *et al.*, 2002).

According to our model, the slip rate on the deep ramp to the north of the Ventura Avenue anticline, which we describe in detail in the following section, should be even greater than that on the Ventura fault and detachment. According to kinematic models of how fault slip changes across fault bends (Suppe, 1983; Shaw *et al.*, 2005), the slip rate on the deep ramp should be significantly higher than that on the detachment and shallow ramp (see Fig. 13 for a schematic illustration). Based on the specific multibend model shown in Figure 12, the slip rate on the deep ramp should be ~1.5 times greater than that on the detachment and Ventura fault ramp, or 6.6–10.5 mm/yr. Some of the slip on the lower portions of the fault is consumed in folding, so only a fraction of the deeper slip appears on the shallower faults. As this deeper ramp lies at the nucleation depth of most large earthquakes, we include this rate in our subsequent hazard assessments.

Regional Structure

Ventura–Pitas Point System

The Ventura fault and anticline continue offshore as the Pitas Point fault across several lateral en echelon offsets, coinciding with a series of anticlines that form traps for oil fields (the Rincon, Carpinteria, and Dos Cuadras fields; Fig. 1) that have been mapped in detail by the oil and gas industry. A 3D seismic dataset across the Dos Cuadras field shows that this structure forms a tight, asymmetric fold that verges to the south. We suggest the Dos Cuadras fold is structurally similar to the Ventura Avenue anticline and

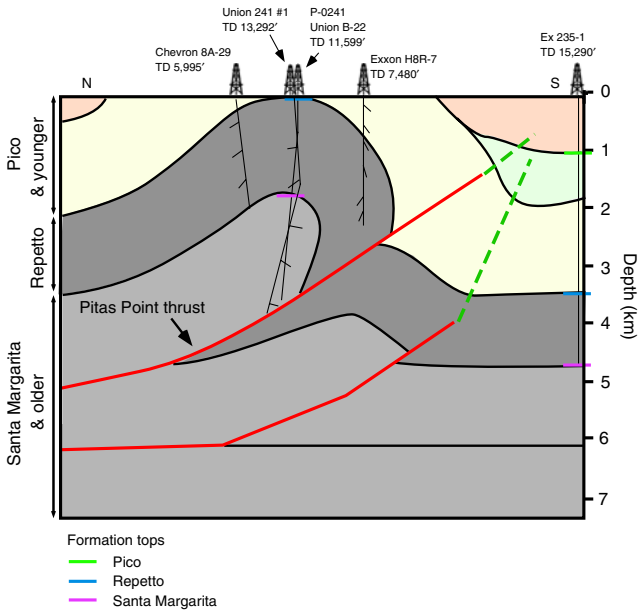

Figure 14. Schematic cross section across the Dos Cuadras anticline showing well control. Geometry is based on a 3D seismic reflection volume (see Fig. 1 for location) and well data (shown here), simplified to depict the most important and continuous structural features of the anticline. Dashed lines show fold axes associated with fault tips. The color version of this figure is available only in the electronic edition.

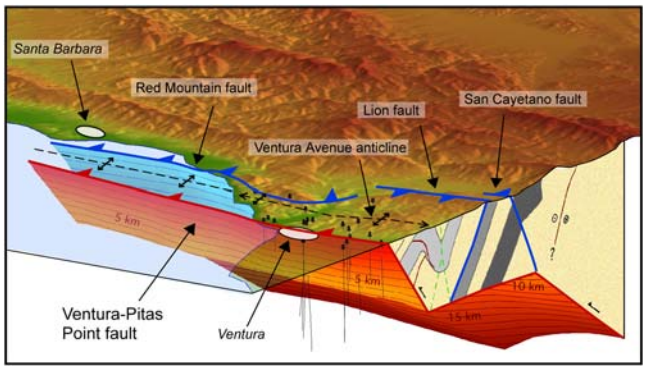

Figure 15. 3D perspective view, from the southeast, of the fault model in the Ventura region. The cities of Ventura and Santa Barbara are identified. The color version of this figure is available only in the electronic edition.

model it also as a fault-propagation fold (Fig. 14). Dos Cuadras is also underlain by a north-dipping thrust fault, known as the Pitas Point thrust. Based on our mapping, the Ventura and Pitas Point faults extend either continuously or en echelon at least 40 km offshore. This is consistent with previous studies that have mapped the Pitas Point fault as an offshore extension of the Ventura fault (e.g., Sarna-Wojcicki *et al.*, 1976; Yeats, 1982a; Yerkes and Lee, 1987; Yerkes *et al.*, 1987; Dahlen, 1989; Kamerling and Nicholson, 1995; Kamerling and Sorlien, 1999; see the USGS fault database, Data and Resources).

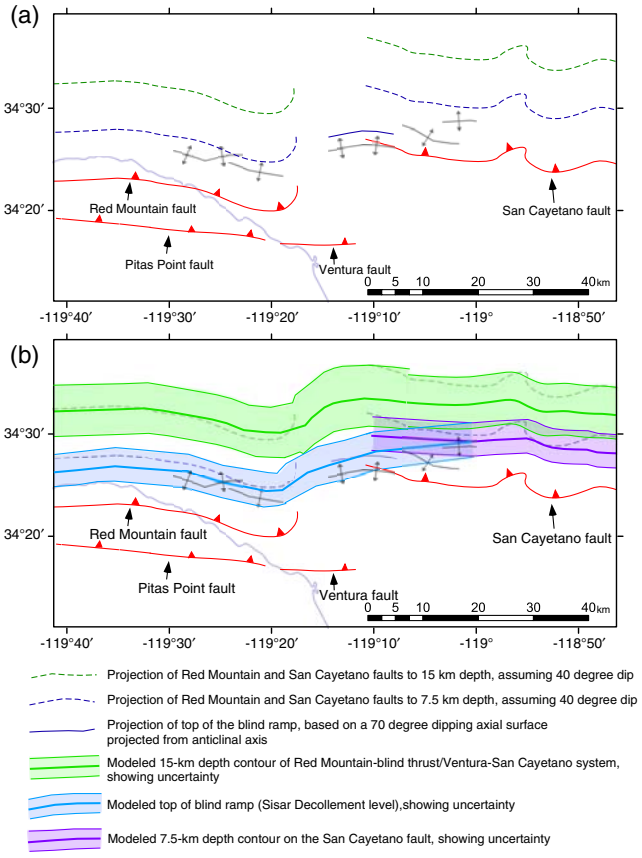

Figure 16. Contours showing connectivity of the north-dipping Red Mountain blind thrust–Ventura–Pitas Point–San Cayetano fault system at depth. (a) Map showing projection to 7.5 and 15 km depth of the San Cayetano and Red Mountain faults, assuming that the faults dip 40°. A projection of the top of the blind ramp north of the Ventura fault is also shown, assuming an axial surface dip of 70°, as depicted in Figure 12. Based on this mapping, the faults appear disconnected from west to east. (b) Contours at 7.5 and 15 km depth extracted from our fault model, with qualitative uncertainties that reflect ±10° dips; in addition, the trace of the top of the axial surface is assumed to have a ±2 km uncertainty. We suggest that the San Cayetano fault merges with the blind thrust at ~119° W longitude and that to the west it forms a hanging wall splay as shown in Figure 15. The color version of this figure is available only in the electronic edition.

The Ventura–Pitas Point fault occupies a special niche in the thrust fault systems that comprise the western Transverse Ranges. Specifically, the fault connects a series of major onshore and offshore fault systems that accommodate significant shortening across the range front. To the east and west of the Ventura fault, the San Cayetano and Red Mountain faults, respectively, accommodate a significant amount of north–south shortening along the range front (Huftile and Yeats, 1995; Huftile *et al.*, 1997). These faults have been mapped as deeply rooted north-dipping faults that likely extend down to the base of seismicity. However, the faults are not directly connected at the surface, leaving a 15 km wide gap at the position of the Ventura fault (Figs. 15 and 16).

Blind Ramp and Lion Backthrust

In this gap, we and others (e.g., Namson, 1987; Huftile, 1988; Namson and Davis, 1988) interpret the existence of a thrust ramp (here termed the blind ramp) that flattens to a detachment, producing the large monoclinal south-dipping fold limb that is exposed north of the Ventura Avenue anticline. Based on fault-bend folding theory (Suppe, 1983), the width of this fold limb implies that the blind thrust has accommodated ~9 km of shortening (Fig. 12). Previous studies (e.g., Huftile and Yeats, 1995) have suggested that all of this shortening reaches the surface along the Lion backthrust, resulting in a structural wedge (Medwedeff, 1989; Shaw *et al.*, 2005). We agree that the bulk of the slip must have occurred on the Lion backthrust but interpret that a component is partitioned onto the Ventura fault (~2.1 km), which rises from the same (Sisar) detachment. Furthermore, we suggest the blind ramp and associated folding may have developed as a fault-propagation fold prior to breaking through onto the Sisar decollement and reaching its current configuration. In this case, a component of the south-dipping monocline would represent the frontlimb of this deeply rooted fault-propagation fold. This interpretation does not alter the slip that we interpret on the Ventura fault beneath the Ventura Avenue anticline, nor the existence of the blind ramp, but would require significantly less cumulative slip on the blind thrust and Lion backthrust.

San Cayetano and Southern San Cayetano Faults

The large, south-dipping fold limb produced by flattening of the blind thrust extends past the eastern edge of the Ventura Avenue anticline, where there is no surface scarp similar to the Ventura fault, and progressively narrows toward the east. Here, the western part of the San Cayetano fault is exposed within the mountains, high above the basin floor (Rockwell, 1988). We suggest that the blind ramp that feeds slip southward onto the Sisar decollement, Lion backthrust, and Ventura fault does not terminate at the eastern edge of the Ventura fault. Rather, it must continue eastward, given the presence and continuity of the south-dipping monoclinal fold limb. We call the structure that is responsible for this fold limb the southern San Cayetano fault (SSCF), because it uplifts material to the south of the San Cayetano fault, including the fault itself. As discussed in the previous paragraph, there are two possible interpretations for the development of this fold limb, with different implications for how slip is consumed east of the Ventura fault. If the monocline is a fault-bend fold, then the SSCF represents an eastward extension of the Lion backthrust into the footwall of the San Cayetano fault, as shown in Figures 17 and 18 (model 1). Alternatively, if the fold limb developed in part by upward propagation of the blind thrust, then the SSCF may similarly represent a north-dipping blind thrust in the footwall of the San Cayetano fault (model 2).

We suggest the western part of the San Cayetano fault may represent a steeper splay rising from the deep blind ramp, whereas the SSCF is linked either directly to the deep thrust ramp (model 2) or is linked as a backthrust via the Sisar decollement (model 1). In either case, slip is partitioned between the two faults (the San Cayetano fault and the SSCF). Toward the east, more and more slip is placed on the San Cayetano fault and the SSCF becomes less important (as shown by the narrowing of the south-dipping monocline), until finally the eastern part of the San Cayetano fault is no longer uplifted by an underlying fault, but rather crops out at the base of the mountain front. This part of the fault has an exceptionally rapid slip rate of at least 7.5 mm/yr, and

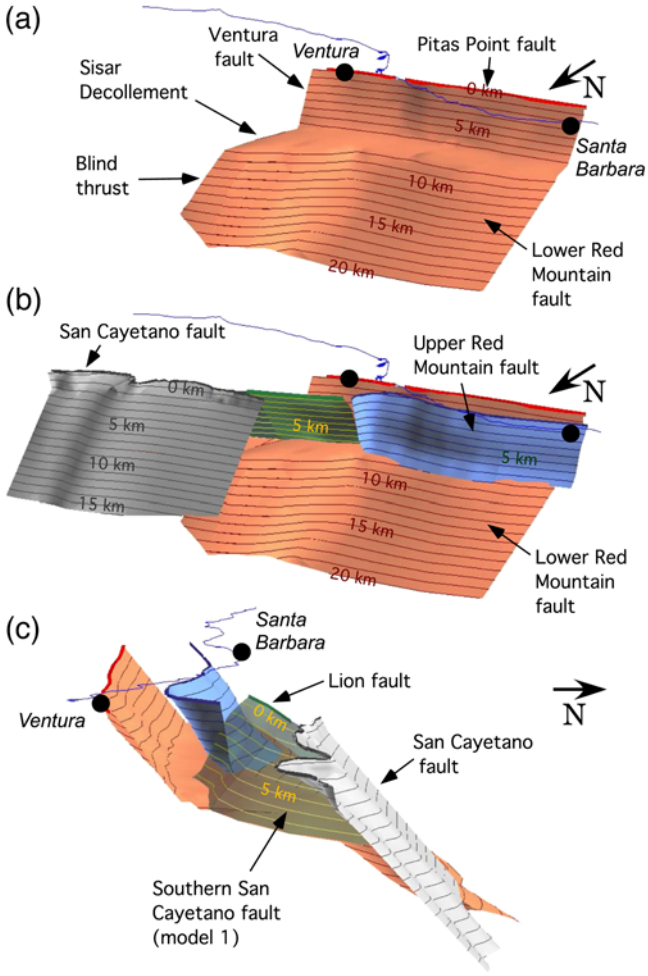

Figure 17. 3D perspective view of the faults in the Ventura region: (a) from the northwest, showing just the Ventura and Pitas Point faults, with the flat and ramp dipping down to the north; (b) from the northwest, showing these same faults in the context of the regional structure; and (c) from the east, with the Lion–SSCF (described in the text) shown as semitransparent. Note that only model 1 of the SSCF is shown here. The San Cayetano fault geometry is taken from the community fault model for southern California (Plesch *et al.*, 2007). The California coastline and the cities of Ventura and Santa Barbara are shown as a thin line and solid circles, respectively. A rupture of just the Ventura–Pitas Point fault with their deeper extents (the blind thrust and the lower Red Mountain fault) could generate an earthquake of M_w 7.5. The color version of this figure is available only in the electronic edition.

may slip as fast as ~10 mm/yr—the fastest rate documented for any fault in the Transverse Ranges (Huftile and Yeats, 1995; Dolan and Rockwell, 2001; Nicholson *et al.*, 2007). In contrast, the slip rate of the western part of the fault is slower than the eastern segment, and diminishes westward to zero (Rockwell *et al.*, 1984). We suggest this decrease in slip reflects the portioning of slip onto the SSCF.

The SSCF is a new, previously unmapped fault, and no fault trace has been identified, either because it does not reach the surface (model 2) or because the surface trace is obscured by the San Cayetano fault (model 1). However, we can see evidence for the activity of the SSCF along the synclinal axis of the monocline that it produces. To the east of the Ventura Avenue anticline and fault, this syncline occurs along the range front. Boreholes excavated along the range front indicate that the syncline folds late Pleistocene and Holocene strata, suggesting that the underlying SSCF at this location is active (McAuliffe *et al.*, 2011).

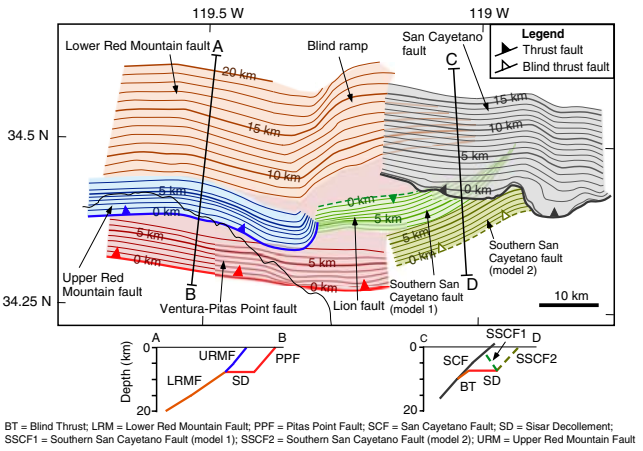

Figure 18. (Top) Contour map of the faults in the Ventura region. Note that we depict two alternative interpretations for the SSCF (models 1 and 2; discussed in the text). (Bottom) Schematic cross sections (AB and CD) illustrating the fault geometries to the west and east of the Ventura fault. The color version of this figure is available only in the electronic edition.

Red Mountain Fault

To the west of the Ventura Avenue anticline, we suggest that the Red Mountain fault is structurally similar to the San Cayetano fault (Yeats *et al.*, 1988; Huftile and Yeats, 1995), in that it rises from a deep thrust ramp that also feeds slip to the south onto the Pitas Point fault. Here, we divide the Red Mountain fault into two parts: the lower and upper parts, below and above the level of the Sisar decollement, respectively. This has been done so as to allow us to distinguish between different rupture scenarios, as a rupture on the lower Red Mountain fault might propagate south onto the Sisar decollement–Pitas Point thrust or upward onto the upper Red Mountain fault.

Like with the Ventura fault, uplifted terraces provide information about the slip history of the Red Mountain and Pitas Point faults. Huftile *et al.* (1997) examined the uplifted Punta Gorda terrace, which lies near the coast, north of the eastern tip of the Pitas Point fault. This terrace intersects the south strand of the Red Mountain fault and shows that over the last 45 ka the footwall of the Red Mountain fault rose at a rate of ~4.6 mm/yr, whereas the hanging wall rose an additional ~1.1 mm/yr. This strand of the Red Mountain fault roughly coincides with a mapped syncline that lies directly to the north of Rincon anticline, which is the product of slip on the Pitas Point fault (Dibblee and Ehrenspeck, 1988). We therefore believe the footwall uplift is due to slip on the Pitas Point fault, whereas the additional hanging wall uplift represents slip on the southern strand of the upper Red Mountain fault. Thus, we interpret a slip rate of 5.6–6.5 mm/yr on the Pitas Point fault (assuming a fault dip of 45°–55°) and a slip rate of 1.3–1.6 mm/yr on the south strand of the Red Mountain fault (assuming a fault dip of 45°–55°) for a combined fault slip rate of ~9.5–11.1 mm/yr on the lower Red Mountain fault. (The excess slip on the deep ramp is consumed by folding, as described at the end of the Slip and Activity of the Ventura Fault section and Fig. 13.) This implied slip rate on the Pitas Point fault system (5.6–6.5 mm/yr on the upper part, 9.5–11.1 mm/yr on the deep ramp) is indistinguishable from the rate that we interpret for the Ventura fault system (4.4–6.9 mm/yr on the upper part, 6.6–10.5 mm/yr on the deep ramp), indicating there is likely continuity in slip rate as well as geometry across the Ventura–Pitas Point fault junction. The study of Huftile *et al.* (1997) describes multiple strands of the Red Mountain fault in this region but only examines the uplift rate across the southern strand. Taking the middle or northern strands into account would increase the interpreted slip rate on the lower Red Mountain fault.

Potential for Structural Connectivity

The San Cayetano, Red Mountain, Lion, and Ventura–Pitas Point faults have separate surface traces, and simple projections of these faults to depth at constant dip angles would not allow for structural connectivity. However, we suggest that they may be connected structurally in the subsurface, and have developed a reasonable 3D structural model that demonstrates the faults may merge at depth (Fig. 16). Specifically, we suggest that the blind ramp lying north of the Ventura fault and Sisar decollement may form a continuous connection between the Red Mountain and the San Cayetano faults (Figs. 16–18). To the west, this deep thrust is interpreted to extend upward and daylight as the Red Mountain fault; to the east, the San Cayetano fault forms a steeper splay that rises from the deep ramp and finally merges into it further east at a longitude of ~119 °W (Fig. 17). At the location of the Ventura Avenue anticline, it does not break through, but rather the faulting extends southward; slip is partitioned between the Lion backthrust and the Ventura fault.

Table 3
Published Empirical Equations Relating Earthquake Magnitude, Fault Area, and Average Displacement

Reference	Relation	Equation Number
Hanks and Bakun (2002, 2008)	$M_w = 3.98 + \log(A)$, for $A \lesssim 537$	(1)
	$M_w = 3.07 + 4/3 \log(A)$, for $A > 537$	(2)
Biasi and Weldon (2006)	$M_w = 6.92 + 1.14 \log(d_{ave})$	(3)

M_w, earthquake magnitude; A, fault area in km^2; d_{ave} = average displacement (in m). These equations incorporate the data of Wells and Coppersmith (1994).

Table 4
Possible Single- and Multisegment Rupture Scenarios

Fault Segments	A (km^2)	M_w	d_{ave} (m)	Recurrence Interval (years)
V	122	6.1	0.12	17–27
V+PP	446.2	6.6	0.53	76–120
V+BR	705.5	6.9	0.90	81–205
V+BR+SC	1589.5	7.3	2.33	210–530
V+PP+BR+LRM	2083.5	7.5	3.19	287–725
V+PP+BR+LRM+SC	2967.5	7.7	4.83	435–1098
V+PP+BR+LRM+URM+SC	3391.8	7.8	5.65	509–1284

V, Ventura; PP, Pitas Point; BR, blind ramp; SC, San Cayetano; LRM, lower Red Mountain; URM, upper Red Mountain. Note that magnitude is calculated using equations (1) and (2), and the average displacement is calculated using equation (3) (Table 3). The recurrence interval is calculated using slip rates of 4.4–6.9 for the Ventura fault, 6.6–10.5 for the deep, blind ramp, 5.6–6.5 on the Pitas Point fault, and 9.5–11.1 mm/yr on the lower Red Mountain fault. The first two scenarios use ranges of 4.4–6.9 mm/yr, whereas the remainder use inclusive ranges of 4.4–11.1 mm/yr, based on the faults being considered. Note that we do not have any historical records of rupture on these faults, suggesting that the system tends to rupture in multisegment events (based on the recurrence intervals).

Seismic Hazard

Rupture Scenarios for Single- and Multisegment Events

Our interpretation of the Ventura fault as a deeply rooted, active structure with a high slip rate suggests that it poses a considerable seismic hazard. Moreover, we suggest that the fault system may be connected to a larger system of faults. These include the Pitas Point fault along strike and the Red Mountain, San Cayetano, and SSC faults across strike that connect to the Ventura–Sisar–blind ramp at depth (Figs. 16–18) (Huftile, 1988; Huftile and Yeats, 1995; Plesch *et al.*, 2007). Despite the apparent disconnected nature of these faults at the surface, our 3D model indicates they may link together below 7.5 km and form a nearly continuous fault surface. Thus, in order to properly characterize the potential hazards of the Ventura fault, we must consider a wide range of single- and multisegment rupture scenarios.

Our 3D fault model allows us to calculate the fault areas for possible ruptures and thereby estimate the maximum earthquake magnitudes that could occur on these faults using published empirical relations (Table 3; Hanks and Bakun, 2002, 2008; Biasi and Weldon, 2006). These relations allow us to speculate about the potential maximum earthquake magnitudes and potential recurrence intervals for these earthquakes. These maximum magnitudes are not necessarily the only possible rupture scenarios but serve as a basis for examining the range of potential earthquake magnitudes.

The area of the modeled Ventura fault, together with its down-dip extent to the north on the blind ramp, is 705 km^2, which could yield an earthquake of magnitude 6.9. This represents a considerable seismic hazard, given that the fault would rupture through downtown Ventura. If this represents the characteristic earthquake for this system, it should occur with a recurrence interval of ~8–200 years (Table 4). If, instead, the Ventura fault typically ruptured alone, earthquakes would be smaller (~M_w 6.1) but much more frequent (every 20–30 years), which is not supported by the historical record.

A much greater threat is posed by the prospect of a multisegment rupture, in which the Ventura fault connects along strike to the Pitas Point fault or down-dip to the San Cayetano and lower Red Mountain faults (Table 4). If the Ventura and Pitas Point faults ruptured together with their down-dip extents, the estimated earthquake magnitude could reach M_w 7.5; a rupture incorporating these faults together with full ruptures of the Red Mountain and San Cayetano faults could produce a much larger (M_w 7.8) event. Recent earthquakes have demonstrated that thrust systems can indeed rupture multiple fault segments, including detachments, resulting in large and damaging events (e.g., M_w 7.9 Wenchuan earthquake, China: Hubbard *et al.*, 2010, Qi *et al.*, 2011; M_w 7.6 Chi-Chi earthquake, Taiwan: Yue *et al.*, 2005).

We can estimate the average displacements and recurrence intervals of such earthquakes. For these estimates, we consider the slip rate estimates that we have determined for each fault in the system, as described in Table 4. For the faults for which we have generated 3D models, the calculated recurrence intervals range from tens to over one thousand years, with increasing intervals for larger earthquakes. No historical earthquakes have been observed on the Ventura fault; this suggests that recurrence intervals on the fault are likely toward the higher end of the range, implying that the Ventura fault tends to rupture in larger, multisegment events.

Paleoseismic Evidence for Rupture Magnitude

A recent study by Rockwell (2011) using vintage aerial photography has identified a series of emergent Holocene terraces, some originally recognized by Lajoie *et al.* (1982), along the coast on the Ventura Avenue anticline that appear to represent episodic uplift events. These terraces, which date

Table 5
Average Displacement Estimates for Events on the Ventura Fault, Based on Rockwell (2011) Uplifted Terraces

Source	Slip estimate
Estimate of average uplift on Holocene terraces of 4–7 m (Rockwell, 2011), combined with 45° fault dip and kinematic model of Ventura fault.	~5.7–9.9 m
Maximum measured uplift of Holocene terraces (10 m; Rockwell, 2011), combined with 45° fault dip and kinematic model of Ventura fault; based on the idea that slip recorded at the surface is generally less than 2× average, sometimes up to 3× average (e.g., Biasi and Weldon, 2006).	4.7–7.1 m or more
Recurrence interval: Time between terraces 1100–1600 years. Apply slip rate of 5.6–6.5 mm/yr, which represents the overlap in slip rates calculated for the Ventura and Pitas Point faults.	6.2–10.7 m
Total range considered (inclusive)	4.5–10.7 m
Most likely range (overlap)	6.2–9.9 m

to ~800, 1900, 3500, and 5000 years ago, show 5–10 m of uplift per event, suggesting the fault system must slip in large events. We note that these uplift measurements are taken locally, whereas empirical relationships that relate slip to earthquake magnitude rely on the average displacement in an event. We therefore apply three distinct methods that take into account slip variability along the fault to convert these local uplift measurements to average displacement (Table 5). These three methods produce similar ranges of values, so we take both the full range and suggest that the average slip in these events is likely between 4.5 and 10.7 m (Table 5). We recognize, however, that there may be additional factors that could lead to anomalously high uplift, such as local faulting beneath the terraces.

Using this estimate of average displacement (4.5–10.7 m), we apply equations (2) and (3) from Table 3 to estimate the magnitude and rupture area required to produce the uplift recorded by the terraces (Table 6). By comparing this required rupture area with the rupture scenarios in Table 4, we determine that such a rupture could be accomplished by involving nearly all of the faults that we have identified in this study related to the Ventura–Pitas Point system (Table 4). Other faults in the western Transverse Ranges might also be included in such a rupture, like the Red Mountain fault west of our study area. Alternatively or in addition, such ruptures may involve the Santa Susana and/or the Sierra Madre faults, north-dipping faults that lie along strike to the east of our study area. Like the Ventura system, surficial discontinuity of these structures may also mask structural linkage at depth. A rupture of this nature would have an expected recurrence interval of 370–2430 years (Table 6), which is consistent with the time gaps between terraces of 1100 and 1600 years identified by Rockwell (2011). The latest event appears to have occurred ~800 years ago, placing us within a time range when another event might be expected.

Table 6
Earthquake Scenarios Required to Produce Uplift Recorded by Terraces (Rockwell, 2011)

	d_{ave} (m)	M_w	A (km^2)	Recurrence Interval (years)
Smallest event	4.5	7.7	2800	370–1020
Most likely smallest event	6.2	7.8	3700	510–1410
Most likely largest event	9.9	8.1	5480	810–2250
Largest event	10.7	8.1	5820	880–2430

d_{ave} is estimated from the terrace uplifts (Table 5). M_w and A are calculated using d_{ave} and equations (2) and (3) from Table 3. The recurrence interval is calculated using d_{ave} and the slip rate that we estimate in this study (4.4–12.2 mm/yr; see discussion in Table 4 caption).

Conclusions

The western Transverse Ranges are underlain by a set of east–west-trending north-dipping reverse faults that extend to seismogenic depth. Some of these faults, including the Red Mountain fault to the west and the San Cayetano fault to the east of the Ventura area, accommodate significant amounts of shortening. We show that these faults may be linked laterally by a blind ramp. In the Ventura area and offshore to the west, a north-dipping blind ramp is interpreted, in this and prior studies, to link upward to a decollement, at ~7.4 km.b.s.l., that extends southward and connects to the Ventura–Pitas Point thrust system. This system extends at least 50 km east–west, passing through the city of Ventura and beneath the city of Santa Barbara.

Measures of displacement on the Ventura fault suggest the Ventura Avenue anticline grew as a fault-propagation fold, because slip decreases upward toward the surface. Uplifted terraces indicate the anticline rose at 9–25 mm/yr from 200 to 300 ka to 105 or 80 ka, 3–14 mm/yr from 105 or 80 ka to ~30 ka, and 3–7 mm/yr from ~30 ka to the present (Rockwell *et al.*, 1988). We suggest that the decrease in uplift rate over time may have been related to a breakthrough of the Ventura fault to the surface at 30 ± 10 ka. Because of this breakthrough, the structural behavior of the system changed from fault propagation to fault-bend folding, which would cause the uplift rate to decrease by a factor of 2 while maintaining a constant shortening rate.

Our interpretation of the above composite history of the Ventura Avenue anticline and Ventura fault allows us to convert uplift rates on terraces (Rockwell *et al.*, 1988; Huftile *et al.*, 1997) into a slip rate on the fault. Based on this analysis, we conclude that the Ventura–Pitas Point fault appears to slip at a rate of 4.4–6.9 mm/yr, with higher rates up to

11.1 mm/yr on the deeper ramps to the north. This rate is consistent with GPS data, which show significant north–south shortening across this part of the Transverse Ranges (7–10 mm/yr; Donnellan *et al.*, 2002).

We construct a 3D fault model of the western Transverse Ranges, linking the Ventura–Pitas Point fault to the Red Mountain fault to the west and to the San Cayetano fault to the east. This fault geometry may allow ruptures to propagate very long distance along strike, producing large, multisegment events (M_w 7.3–7.8 or greater). Indeed, it appears unlikely that many of the faults in the system rupture in smaller, single-segment events (M_w 6.1–6.6), given that the high slip rate would require such earthquakes to occur one to seven times every 100 years, a behavior that is not visible in the historical record. This conclusion is further supported by new evidence from uplifted Holocene terraces, which shows the Ventura Avenue anticline likely rises in discrete events with 5–10 m of uplift, requiring an earthquake of $\sim M_w$ 7.7–8.1 every 400–2400 years, with the latest event ~800 years ago (Table 5; Rockwell, 2011).

This analysis reinforces the importance of 3D structural analyses for understanding seismic hazards. As observed in the 2008 M_w 7.9 Wenchuan earthquake, earthquakes are capable of rupturing multiple imbricate faults in a single event, in addition to jumping large lateral segment boundaries (Hubbard and Shaw, 2009; Hubbard *et al.*, 2010). This capability is likely derived in large part from the connectivity of fault systems at depth. Such connectivity is expected in fold-and-thrust belts around the world, both on land (e.g., Himalaya, Bangladesh, western Taiwan) and offshore (e.g., Sumatran subduction zone, Aleutian trench, Japan trench). Our analysis shows the Ventura–Pitas Point system is a fault system where splays appear disconnected at the surface but may link into a nearly continuous source at seismogenic depths. Ground motions from a large rupture on the Ventura–Pitas Point fault system would undergo significant amplification due to the deep sediments of the Ventura basin. Shaking could also be amplified in the nearby Los Angeles and San Fernando basins (Field, 2000; 2001). In addition, a rupture of the Pitas Point fault with 5–10 m of uplift could produce a strong tsunami. Quantifying these hazards is of immediate importance, given that we interpret a recurrence interval on this fault of ~400–2400 years, with the last two events occurring ~800 and 1900–2000 years ago.

Data and Resources

The seismic reflection line VB1 was provided courtesy of Texaco, Inc. The 3D Dos Cuadras seismic dataset was acquired by Texaco, Inc., in 1983 and is now available to the public via the Bureau of Ocean Energy, Management, Regulation and Enforcement.

Well data were taken from the database provided by the California Department of Conservation website, Division of Oil, Gas, and Geothermal Resources, publicly available at http://www.conservation.ca.gov/dog/ (last accessed September 2011).

Acknowledgments

Thanks to Chris Cothrun, Ben Haravitch, Zurriya Hasnan, Samuel Rosenbaum, and Rachel Zucker for their assistance in the field acquiring seismic data. We thank Chandra Shaker (City of Ventura) and Anitha Balan (Ventura County) for helping us obtain permits for seismic acquisition and Gary Brummet, Dorcas Thille, and Dave Pommer for allowing us to acquire seismic reflection data on private property. We also thank Amanda Hughes, Craig Nicholson, and Andrew Rhines for their helpful discussions and Phil Hogan (Fugro) and Drew Mayerson (Bureau of Ocean Energy, Management, Regulation and Enforcement) for helping us acquire a copy of the Dos Cuadras seismic reflection data. We appreciate the help of Kate Scharer, Gary Fuis, and Patricia McCrory for providing internal United States Geological Survey (USGS) reviews and the help of Mike Oskin and an internal reviewer for assessing the manuscript through the *BSSA*. We thank the Southern California Earthquake Center and its funding agencies for providing funding for this study through Proposal Number 10201.

References

Adams, J. T., J. K. Ayodele, J. Bedford, C. H. Kaars-Sijpesteijn, and N. L. Watts (1992). Application of dipmeter data in structural interpretation, Niger delta, *Spec. Publ. Geol. Soc. Lond.* **65,** 247–263.

Allmendinger, R. W. (1998). Inverse and forward numerical modeling of trishear fault-propagation folds, *Tectonics* **17,** 640–656.

Biasi, G. P., and R. J. Weldon (2006). Estimating surface rupture length and magnitude of paleoearthquakes from point measurements of rupture displacement, *Bull Seismol. Soc. Am.* **96,** 1612–1623.

Brankman, C. M. (2009). Three-dimensional structure of the western Los Angeles and Ventura basins, and implications for regional earthquake hazard, *Ph.D. Thesis*, Harvard University, Cambridge, Massachusetts.

California Department of Oil, Gas, and Geothermal Resources (Editor) (1997). California Oil and Gas Statistics, *2007 Annual Report*, ftp://ftp.consrv.ca.gov/pub/oil/annual_reports/2007/PR06_2007.pdf (last accessed August 2011).

Chester, J. S., and F. M. Chester (1990). Fault-propagation folds above thrusts with constant dip, *J. Struct. Geol.* **12,** no. 7, 903–910.

Clark, M. M., K. H. Harms, J. J. Lienkaemper, D. S. Harwood, K. R. Lajoie, J. C. Matti, J. A. Perkins, M. J. Rymer, A. M. Sarna-Wojcicki, R. V. Sharp, J. D. Sims, J. C. Tinsley III, and J. I. Ziony (1984). Preliminary slip rate table and map of late Quaternary faults of California, *U.S. Geol. Surv. Open-File Rept. 84-106*.

Dahlen, M. Z. (1989). Late Quaternary history of the Ventura mainland shelf, California: Implications for late Pleistocene sea level, *GSA Abstr. Programs* **21,** no. 5, 71.

DeVecchio, D. E., R. V. Heermance, M. Fuchs, and L. A. Owen (2012). Climate-controlled landscape evolution in the western Transverse Ranges, California: Insights from Quaternary geochronology of the Saugus Formation and strath terrace flights, *Lithosphere* **4,** no. 2, 110–130, GSA Data Repository Item 2012077, doi: 10.1130/L176.1.

Devilliers, M. C., and Ph. Werner (1990). Example of fault identification using dipmeter data, *Spec. Publ. Geol. Soc. Lond.* **48,** 287–295.

Dibblee, T. W. and H. E. Ehrenspeck (Editors) (1988). Geologic map of the Ventura and Pitas Point quadrangles, Ventura County, California, Vol. DF-21, *Dibblee Geological Foundation*, scale 1:24000.

Dibblee, T. W. and H. E. Ehrenspeck (Editors) (1992). Geologic map of the Saticoy quadrangles, Ventura County, California, Vol. DF-42, *Dibblee Geological Foundation*, scale 1:24000.

Dolan, J. F., and T. K. Rockwell (2001). Paleoseismologic evidence for a very large ($M_w > 7$), post-A.D. 1660 surface rupture on the eastern San Cayetano fault, Ventura County, California: Was this the elusive source of the damaging 21 December 1812 earthquake? *Bull. Seismol. Soc. Am.* **91,** no. 6, 1417–1432.

Donnellan, A., J. W. Parker, and G. Peltzer (2002). Combined GPS and InSAR models of postseismic deformation from the Northridge earthquake, *Pure Appl. Geophys.* **159,** 2261–2270.

Erslev, E. A. (1991). Trishear fault-propagation folding, *Geology* **19,** no. 6, 617–620.

Field, E. H. (2000). A modified ground-motion attenuation relationship for southern California that accounts for detailed site classification and a basin-depth effect, *Bull. Seismol. Soc. Am.* **90,** no. 6B, S209–S221, doi: 10.1785/0120000507.

Field, E. H. (2001). Earthquake ground-motion amplification in southern California, Poster provided by the Southern California Earthquake Center; available at http://www.scec.org/news/01news/news010828b.html (last accessed February 2013).

Hanks, T. C., and W. H. Bakun (2002). A bilinear source-scaling model for **M** – log *A* observations of continental earthquakes, *Bull. Seismol. Soc. Am.* **92,** 1841–1846.

Hanks, T. C., and W. H. Bakun (2008). **M** – log *A* observations for recent large earthquakes, *Bull. Seismol. Soc. Am.* **98,** no. 1, 490–494.

Hardy, S., and M. Ford (1997). Numerical modeling of trishear fault-propagation folding and associated growth strata, *Tectonics* **16,** no. 5, 841–854.

Hubbard, J., and J. H. Shaw (2009). Uplift of the Longmen Shan and Tibetan plateau, and the 2008 Wenchuan (M = 7.9) earthquake, *Nature* **458,** 194–197.

Hubbard, J., J. H. Shaw, and Y. Klinger (2010). Structural setting of the 2008 M_w 7.9 Wenchuan, China, earthquake, *Bull. Seismol. Soc. Am.* **100,** 2713–2735.

Huftile, G. J. (1988). Subsurface connection between the Red Mountain and San Cayetano faults, Ventura basin, California (abstract), *Eos Trans. AGU* **69,** no. 1419.

Huftile, G. J., and R. S. Yeats (1995). Convergence rates across a displacement transfer zone in the western Transverse Ranges, Ventura Basin, California, *J. Geophys. Res.* **100,** no. B2, 2043–2067.

Huftile, G. J., S. C. Lindvall, L. Anderson, L. D. Gurrola, and M. A. Tucker (1997). Paleoseismic investigation of the Red Mountain fault: Analysis and trenching of the Punta Gorda terrace, *SCEC Progress Report*; available at http://www.scec.org/research/97research/97huftilelindvalletal.html (last accessed February 2013).

Hughes, A. N., and J. H. Shaw (2014). Fault displacement-distance relationships as indicators of contractional fault-related folding style, *Am. Assoc. Pet. Geol. Bull.* **98,** no. 2, 227–251, doi: 10.1306/05311312006.

Jamison, W. R. (1987). Geometric analysis of fold development in overthrust terranes, *J. Struct. Geol.* **9,** no. 2, 207–219.

Kamerling, M. J., and C. Nicholson (1995). The Oak Ridge Fault and fold system, eastern Santa Barbara Channel, California, *SCEC Annual Report*, Vol. II.

Kamerling, M. J., and C. C. Sorlien (1999). Quaternary slip and geometry of the Red Mountain and Pitas Point-North Channel faults, California (abstract), *Eos. Trans. AGU* **80,** no. 46, 1003.

Lajoie, K. R., D. J. Ponti, C. L. Powell, A. Mathieson, and A. M. Sarna-Wojcicki (1991). Emergent marine strandlines and associated sediments, coastal California; A record of Quaternary sea-level fluctuations, vertical tectonic movements, climatic changes, and coastal processes, in *The Geology of North America*, R. B. Morrison (Editor), Vol. K-2, Quaternary Nonglacial Geology, Conterminous U. S., Geol. Soc. Am., 190–214.

Lajoie, K. R., A. M. Sarna-Wojcicki, and R. F. Yerkes (1982). Quaternary chronology and rates of crustal deformation in the Ventura area, in *Neotectonics of Southern California*, Geol. Soc. Am., Cord. Sec., Field Trip Guidebook, 43–51.

Mallet, J. L. (1992). Discrete smooth interpolation in geometric modeling, *Comput. Aided Des.* **24,** 178–191.

McAuliffe, L., J. Dolan, T. Pratt, J. Hubbard, and J. H. Shaw (2011). Characterizing the recent behavior and earthquake potential of the blind western San Cayetano and Ventura fault systems, *Eos Trans. AGU*, (Fall Meet.), San Francisco, California, 5–9 December, Abstract T11A-2279.

Medwedeff, D. A. (1989). Growth fault-bend folding at southeast Lost Hills, San Joaquin Valley, California, *AAPG Bulletin* **73,** 54–67.

Mitra, S. (1990). Fault-propagation folds: Geometry, kinematic evolution and hydrocarbon traps, *AAPG Bulletin* **74,** 921–945.

Mosar, J., and J. Suppe (1992). Role of shear in fault-propagation folding, in *Thrust Tectonics*, K. R. McClay (Editor), Chapman and Hall, London, 123–132.

Namson, J. (1987). Structural transect through the Ventura basin and western Transverse Ranges, in *Structural Evolution of the Western Transverse Ranges, Guidebook 48A. Pacific Section*, T. L. Davis (Editor), Society Economic Paleontologists and Mineralogists, Los Angeles, California, 29–41.

Namson, J., and T. Davis (1988). Structural transect of the western Transverse Ranges, California: Implications for lithospheric kinematics and seismic risk evaluation, *Geology* **16,** 675–679.

Nichols, D. R. (1974). Surface faulting, in *Seismic and Safety Elements of the Resources Plan and Program*, Ventura County Planning Department, 1–35, section 11.

Nicholson, C., M. J. Kamerling, C. C. Sorlien, T. E. Hopps, and J.-P. Gratier (2007). Subsidence, compaction, and gravity sliding: Implications for 3D geometry, dynamic rupture, and seismic hazard of active basin-bounding faults in southern California, *Bull. Seismol. Soc. Am.* **97,** no. 5, 1607–1620.

Ogle, B. A., and R. N. Hacker (1969). Cross section coastal area Ventura County, in *Geology and Oil Fields of Coastal Areas, Ventura and Los Angeles Basins, California*, Pacific Section AAPG, SG, and SEPM, *44th Annual Meeting Field Trip*, Guidebook.

Perry, S. S., and W. A. Bryant (compilers) (2002). Fault number 91, Ventura fault, in *Quaternary fault and fold database of the United States: U.S. Geological Survey website*, available at http://earthquakes.usgs.gov/hazards/qfaults (last accessed May 2011).

Plesch, A., J. H. Shaw, C. Benson, W. A. Bryant, S. Carena, M. Cooke, J. Dolan, G. Fuis, E. Gath, L. Grant, E. Hauksson, T. Jordan, M. Kamerling, M. Legg, S. Lindvall, H. Magistrale, C. Nicholson, N. Niemi, M. Oskin, and S. Perry (2007). Community fault model (CFM) for southern California, *Bull. Seismol. Soc. Am.* **97,** no. 6, 1793–1802, doi: 10.1785/0120050211.

Putnam, W. C. (1942). Geomorphology of the Ventura region, California, *GSA Bulletin* **53,** 691–754, 5 plates.

Qi, W., Q. Xuejun, L. Qigui, J. Freymueller, Y. Shaomin, X. Caijun, Y. Yonglin, Y. Xinzhao, T. Kai, and C. Gang (2011). Rupture of deep faults in the 2008 Wenchuan earthquake and uplift of the Longmen Shan, *Nature Geosci.* **4,** 634–640.

Quick, G. L. (1973). Preliminary microzonation for surface faulting in Ventura, California area, in *Geology, Seismicity, and Environmental Impact*, D. E. Moran, J. E. Slosson, R. O. Stone, and C. A. Yelverton (Editors), Assoc. Engineering Geologists, 257–262, special publication.

Rockwell, T. K. (1988). Neotectonics of the San Cayetano fault, Transverse Ranges, California, *GSA Bulletin* **100,** 500–513.

Rockwell, T. K. (2011). Large co-seismic uplift of coastal terraces across the Ventura Avenue anticline: Implications for the size of earthquakes and the potential for tsunami generation, Plenary talk, in *SCEC Annual Meeting*, Palm Springs, California, 12 September 2011.

Rockwell, T. K., E. A. Keller, M. N. Clark, and D. L. Johnson (1984). Chronology and rates of faulting of Ventura River terraces, California, *GSA Bulletin* **95,** 1466–1474.

Rockwell, T. K., E. A. Keller, and G. R. Dembroff (1988). Quaternary rate of folding of the Ventura Avenue anticline, western Transverse Ranges, southern California, *GSA Bulletin* **100,** 850–858.

Sarna-Wojcicki, A. M., and R. F. Yerkes (1982). Comment on article by R. S. Yeats entitled "Low-shake faults of the Ventura Basin, California", in *Neotectonics in Southern California*, J. D. Cooper (Editor), Geological Society of America, *78th Cordilleran Section Annual Meeting*, Guidebook, 17–19.

Sarna-Wojcicki, A. M., K. M. Williams, and R. F. Yerkes (1976). Geology of the Ventura Fault, Ventura County, California, *U.S. Geological*

Survey Miscellaneous Field Studies, map MF-781, 3 sheets, scale 1:6000.

Scharer, K. M., D. W. Burbank, J. Chen, and R. J. Weldon (2006). Kinematic models of fluvial terraces over active detachment folds: Constraints on the growth mechanism of the Kashi-Atushi fold system, Chinese Tian Shan, *Geol. Soc. Am. Bull.* **118,** nos. 7/8, 1006–1021.

Shaw, J. H., C. Connors, and J. Suppe (2005). *Seismic Interpretation of Contractional Fault-related Folds: An AAPG Seismic Atlas*. Am. Assoc. Pet. Geol., Tulsa, Oklahoma, 157 pp.

Suppe, J. (1983). Geometry and kinematics of fault-bend folding, *Am. J. Sci.* **283,** 684–721.

Suppe, J., and D. A. Medwedeff (1990). Geometry and kinematics of fault-propagation folding, *Eclogae Geol. Helv.* **83,** no. 3, 409–454.

Wehmiller, J. F., K. R. Lajoie, A. M. Sarna-Wojcicki, R. F. Yerkes, G. L. Kennedy, T. A. Stephens, and R. F. Kohl (1978). Amino-acid racemization dating of Quaternary mollusks, Pacific coast, United States, in *4th International Conference on Geochronology, Cosmochronology, Isotope Geology, Short Papers*, Snowmass-at-Aspen, Colorado, 20–25 August, R. E. Zartman (Editor), *U.S. Geol. Surv. Open-File Rept. 78-701*, 445–448.

Wells, D. L., and K. J. Coppersmith (1994). New empirical relationship among magnitude, rupture length, rupture width, rupture area, and surface displacement, *Bull. Seismol. Soc. Am.* **84,** no. 4, 974–1002.

Yeats, R. S. (1982a). Low-shake faults of the Ventura basin, California, in *Neotectonics in Southern California*, J. D. Cooper (Editor), Geological Society of America, *78th Cordilleran Section Annual Meeting*, Guidebook, 3–15.

Yeats, R. S. (1982b). Reply to Sarna-Wojcicki, A. M. and R. F. Yerkes, in *Neotectonics in Southern California*, J. D. Cooper (Editor), Geological Society of America, *78th Cordilleran Section Annual Meeting*, Guidebook, 21–23.

Yeats, R. S. (1983). Large-scale Quaternary detachments in Ventura basin, southern California, *J. Geophys. Res.* **88,** no. B1, 569–583.

Yeats, R. S., G. J. Huftile, and F. B. Grigsby (1988). Oak Ridge fault, Ventura fold belt, and the Sisar decollement, Ventura basin, California, *Geology* **16,** 1112–1116.

Yerkes, R. F., and W. H. K. Lee (1987). Late Quaternary deformation in the western Transverse Ranges, in *Recent Reverse Faulting in the Transverse Ranges*, *U.S. Geol. Surv. Profess. Paper 1339*, 71–82.

Yerkes, R. F., A. M. Sarna-Wojcicki, and K. R. Lajoie (1987). Geology and Quaternary deformation of the Ventura area, in *Recent Reverse Faulting in the Transverse Ranges*, *U.S. Geol. Surv. Profess. Paper 1339*, 169–178.

Yue, L.-F., J. Suppe, and J.-H. Hung (2005). Structure geology of a classic thrust belt earthquake: The 1999 Chi-Chi earthquake Taiwan ($M_w = 7.6$), *J. Struct. Geol.* **27,** 2058–2083.

Department of Earth and Planetary Sciences
Harvard University
20 Oxford Street
Cambridge, Massachusetts 02138
judith.a.hubbard@gmail.com
(J.H., J.H.S.)

Department of Earth Sciences
University of Southern California
Zumberge Hall, ZHS 111
3651 Trousdale Parkway
Los Angeles, California 90089
(J.D., L.M.)

United States Geological Survey
12201 Sunrise Valley Dr. MS 905
Reston, Virginia 20192
(T.L.P.)

Department of Geological Sciences, MC-1020
5500 Campanile Dr.
San Diego State University
San Diego, California 92192-1020
(T.K.R.)

Manuscript received 15 May 2013;
Published Online 6 May 2014